THE ARCHIVE OF MECHANICAL ENGINEERING

VOL. LX 2013 Number 2

10.2478/meceng-2013-0011

Key words: rotation of concentric spheres, fluid sink, slow viscous flow, Stokes approximation

DEEPAK KUMAR SRIVASTAVA [*], *RAJA RAM YADAV* [**], *SUPRIYA YADAV* [***]

STOKES FLOW AROUND SLOWLY ROTATING CONCENTRIC PERVIOUS SPHERES

In this paper, the problem of concentric pervious spheres carrying a fluid sink at their centre and rotating slowly with different uniform angular velocities Ω_1, Ω_2 about a diameter has been studied. The analysis reveals that only azimuthal component of velocity exists and the torque, rate of dissipated energy is found analytically in the present situation. The expression of torque on inner sphere rotating slowly with uniform angular velocity Ω_1, while outer sphere also rotates slowly with uniform angular velocity Ω_2, is evaluated. The special cases like, (i) inner sphere is fixed (i.e. $\Omega_1 = 0$), while outer sphere rotates with uniform angular velocity Ω_2, (ii) outer sphere is fixed (i.e. $\Omega_2 = 0$), while inner sphere rotates with uniform angular velocity Ω_1, (iii.) inner sphere rotates with uniform angular velocity Ω_1, while outer rotates at infinity with angular velocity Ω_2, have been deduced. The corresponding variation of torque with respect to sink parameter has been shown via figures.
AMS subject classification – 76 D07

1. Introduction

Stokes flow is becoming increasingly important due to the miniaturization of fluid mechanical parts e.g., in micromechanics as well as in nanomechanics. Slow rotation of spheroids (including the disc) in an infinite fluid was first solved by **Jeffrey** [1915] using curvilinear coordinates. His approach was later extended to the spherical lens, torus, and other axisymmetric shapes. **Proudman** [1956] and **Stewartson** [1966] analyzed the dynamical properties of a fluid occupying the space between two concentric rotating spheres

[*] *Department of Mathematics; B.S.N.V. Post Graduate College (University of Lucknow, Lucknow); Lucknow-226001, U.P., India; E-mail: dksflow@hotmail.com*

[**] *Department of Mathematics, University of Lucknow, Lucknow (U.P.), India; E-mail: yadav_rr2@yahoo.co.in*

[***] *Department of Mathematics, University of Lucknow, Lucknow (U.P.), India; E-mail: sprya.ydv@rediffmail.com*

when the angular velocities of the spheres are slightly different, in other words, when the motion relative to a reference frame rotating with one of the spheres is due to an imposed azimuthal velocity which is symmetric about the equator. **Kanwal** [1960] has discussed the problem of slow steady rotation of axially symmetric bodies in a viscous fluid. **Rubinow and Keller** [1961] have considered the force on a spinning sphere which is moving through an incompressible viscous fluid by employing the method of matched asymptotic expansions to describe the asymmetric flow. **Brenner** [1961] also obtained some general results for the drag and couple on an obstacle which is moving through the fluid. **Childress** [1964] has investigated the motion of a sphere moving through a rotating fluid and calculated a correction to the drag coefficient. **Wakiya** [1967] numerically evaluated the drag and angular velocity experienced by freely rotating spheres and compared with those calculated from corresponding approximate formulae known before. **Barett** [1967] has tackled the problem of impulsively started sphere rotating with angular velocity Ω about a diameter. He modified the standard time-dependent boundary layer equation to give series solutions satisfying all the boundary conditions and gave solutions that are applicable at small times for non-zero Reynolds numbers. He found that the velocity components decay algebraically rather than exponentially at large distances. **Pearson** [1967] has presented the numerical solution for the time-dependent viscous flow between two concentric rotating spheres. He governed the motion of a pair of coupled non-linear partial differential equations in three independent variables, with singular end conditions. He also described the computational process for cases in which one (or both) of the spheres is given an impulsive change in angular velocity-starting from a state of either rest or uniform rotation. **Majumdar** [1969], has solved, by using bispherical coordinates, the non-axisymmetrical Stokes flow of an incompressible homogeneous viscous liquid in space between two eccentric spheres. It was proved that the resultant force acting upon the spheres is at right angles to the axis of rotation and the line of centres. The effect of the stationary sphere on the force and couple exerted by the liquid on the rotating sphere has been discussed and the results are compared with those of the axisymmetrical case of **Jeffrey** [1915]. **Kanwal** [1970] has considered a disk performing simple harmonic rotary oscillations about its axis of symmetry in a non-conducting viscous fluid which is at rest at infinity. **O'Neill and Majumdar** [1970] have discussed the problem of asymmetrical slow viscous fluid motions caused by the translation or rotation of two spheres. The exact solutions for any values of the ratio of radii and separation parameters are found by them.

Ranger [1971] tackled the problem of axially-symmetric flow past a rotating sphere due to a uniform stream of infinity. He has shown that leading

terms for the flow consists of a linear superposition of a primary Stokes flow past a non-rotating sphere together with an anti symmetric secondary flow in the azimuthal plane induced by the spinning sphere. **Philander** [1971] presented a note on the flow properties of a fluid between concentric spheres. This note concerns the flow properties of a spherical shell of fluid when motion is forced across the equator. The fluid under consideration is contained between two concentric spheres which rotate about a diameter with angular velocity Ω. The consequences of the forcing motion across the equator are explored in his work. **Cooley** [1971] has investigated the problem of fluid motion generated by a sphere rotating close to a fixed sphere about a diameter perpendicular to the line of centres in the case when the motion is sufficiently slow to permit the linearization of the Navier-Stokes equations by neglecting the inertia terms. He used a method of matched asymptotic expansions to find asymptotic expressions for the forces and couples acting on the spheres as the minimum clearance between them tends to zero. In his paper, the forces and couples are shown to have the form $a_0 \ln \varepsilon + a_1 + o(\varepsilon \ln \varepsilon)$, where ε is the ratio of the minimum clearance between the spheres and the radius of the rotating sphere and where a_0 and a_1 are found explicitly. **Munson and Joseph** [1971, part 1 and part 2] have obtained the high order analytic perturbation solution for the viscous incompressible flow between concentric rotating spheres. In second part of their analysis, they have applied the energy theory of hydrodynamic stability to the viscous incompressible flow of a fluid contained between two concentric spheres which rotate about a common axis with prescribed angular velocities. **Riley** [1972] has discussed the thermal effects on slow viscous flow between rotating concentric spheres. **Takagi** [1974a] has considered the flow around a spinning sphere moving in a viscous fluid. He solved the Navier-Stokes equations, using the method of matched asymptotic expansions for small values of the Reynolds number. With the solution, the force and torque on the sphere are computed, and he found that the sphere experiences a force orthogonal to its direction of motion and that the drag is increased in proportion to the square of the spin velocity. **Takagi** [1974b] has studied the Stokes flow for the case in which two solid spheres in contact are steadily rotating with different angular velocities about their line of centres. For the case of two equal spheres, one of which is kept rotating with angular velocity ω while the other is left free, he found that the latter will rotate with angular velocity $\omega/7$. **Munson and Menguturk** [1975, part 3] have studied the stability of flow of a viscous incompressible fluid between a stationary outer sphere and rotating inner sphere theoretically and experimentally. **Wimmer** [1976] has provided some experimental results on incompressible viscous fluid flow in the gap between two concentric rotating spheres. **Takagi** [1977] further studied the problem of steady flow which

is induced by the slow rotation of a solid sphere immersed in an infinite incompressible viscous fluid, on the basis of Navier-Stokes equations. He obtained the solution in the form of power series with respect to Reynolds number. **Drew** [1978] has found the force on a small sphere translating relative to a slow viscous flow to order of the $^1/_2$ power of Re for two different fluid flows far from the sphere, namely pure rotation and pure shear. For pure rotation, the correction of this order to the Stokes drag consists of an increase in the drag. **Kim** [1980] has calculated the torque and frictional force exerted by a viscous fluid on a sphere rotating on the axis of a circular cone of arbitrary vertex angle about an axis perpendicular to the cone axis in the Stokes approximation. **Dennis et al.** [1981] have investigated the problem of viscous incompressible, rotationally symmetric flow due to the rotation of a sphere with a constant angular velocity about a diameter. The solutions of the finite-difference equations are presented for Reynolds number ranging from 1.0 to 5000. **Davis** and **Brenner** [1986] have used the matched asymptotic expansion methods to solve the problem of steady rotation of a tethered sphere at small, non-zero Reynolds numbers. They obtained first order Taylor number correction to both the Stokes-law drag and Kirchhoff's law couple on the sphere for Rossby numbers of order unity. **Gagliardi** [1987] has developed the boundary conditions for the equations of motion for a viscous incompressible fluid in a rotating spherical annulus. The solution of the stream and circumferential functions were obtained in the form of a series of powers of the Reynolds number. Transient profiles were obtained for the dimensional torque, dimensionless angular velocity of the rotating sphere, and the dimensionless angular momentum of the fluid. **Marcus and Tuckerman** [1987, part 1 and 2] have computed numerically the steady and translation simulation of flow between concentric rotating spheres. **O'Neill and Yano** [1988] derived the boundary condition at the surfactant and substrate fluids caused by the slow rotation of a solid sphere which is partially submerged in the substrate fluid. **Yang** et al [1989] have provided the numerical schemes for the problem of the axially symmetric motion of an incompressible viscous fluid in an annulus between two concentric rotating spheres. **Gagliardi** et al. [1990] reported the study of the steady state and transient motion of a system consisting of an incompressible, Newtonian fluid in an annulus between two concentric, rotating, rigid spheres. They solved the governing equations for the variable coefficients by separation of variables and Laplace Transform methods. They presented the results for the stream function, circumferential function, angular velocity of the spheres and torque coefficient as a function of time for various values of the dimensionless system parameters. **Ranger** [1996] has found an exact solution of the Navier-Stokes equations for the axi-symmetric motion (with swirl) rep-

resenting exponentially time-dependent decay of a solid sphere translating and rotating in a viscous fluid relative to a uniform stream whose speed also decays exponentially with time. He also described a similar solution for the two-dimensional analogue where the sphere is replaced by a circular cylinder of infinite length. **Tekasakul** et al. [1998] have studied the problem of the rotatory oscillation of an axi-symmetric body in an axi-symmetric viscous flow at low Reynolds numbers. They evaluated numerically the local stresses and torques on a selection of free, oscillating, axi-symmetric bodies in the continuum regime in an axi-symmetric viscous incompressible flow. **Datta and Srivastava** [2000] have tackled the problem of slow rotation of a sphere with fluid source at its centre in a viscous fluid. In their investigation, it was found that the effect of fluid source at the centre is to reduce the couple on slowly rotating sphere about its diameter. **Kim and Choi** [2002] conducted the numerical simulations for laminar flow past a sphere rotating in the streamwise direction, in order to investigate the effect of the rotation on the characteristics of flow over the sphere.

Tekasakul and Loyalka [2003] have investigated the rotary oscillations of several axi-symmetric bodies in axi-symmetric viscous flows with slip. A numerical method based on the Green's function technique is used and analytic solutions for local stress and torque on spheres and spheroids as function of the frequency parameter and the slip coefficients are obtained. They have analysed that in all cases, slip reduces stress and torque, and increasingly so with the increasing frequency parameter. **Liu** et al. [2004] have developed a very efficient numerical method based on the finite difference technique for solving time-dependent non-linear flow problems. They have applied this method to study the unsteady axisymmetric isotherm flow of an incompressible viscous fluid in a spherical shell with a stationary inner sphere and a rotating outer sphere. **Ifidon** [2004] numerically investigated the problem of determining the induced steady axially symmetric motion of an incompressible viscous fluid confined between two concentric spheres, with the outer sphere rotating with constant angular velocity and the inner sphere fixed for large Reynolds numbers. **Davis** [2006] obtained the expression for force and torque on a rotating sphere close to and within a fluid-filled rotating sphere. **Marcello** [2008] has introduced new exact analytic solutions for the rotational motion of an axially symmetric rigid body having two equal principal moments of inertia and subjected to an external torque which is constant in magnitude. Recently, **Srivastava et al.** [2011] have studied the effect of viscous fluid around slowly rotating sphere with sink at its centre in which they concluded that the effect of sink at the centre is to reduce the couple.

In the present paper, the problem of slow rotation of concentric spheres, both assumed to be pervious, with a sink at their centre has been tackled. If

the strength '-Q' of the sink were of the same order as the angular velocity Ω of rotating spheres, the inertia terms could still be neglected, and the total flow then consists of only the source solution superimposed on the Stokes solution. Therefore, in this case the Stokes drag and torque are not affected by the sink. Also, if Q is large enough so that $Q\Omega$ is not negligible, the inertia terms, being non-linear, cannot be altogether omitted. The Navier-Stokes equation, can still be linearized by assuming that the velocity perturbation in the source flow on account of the Stokes flow is small, so that the terms containing square of angular velocity (i.e. of order Ω^2) can be neglected. This assumption is justifiable at least in the vicinity of the spheres where the Stokes approximation is valid. The present problem corresponds to the problem of Stokes flow past a sphere with source at its centre investigated by **Datta** [1974] and slow rotation of sphere with source at its centre in a viscous fluid investigated by **Datta & Srivastava** [2000], **Srivastava et al.** [2011], the results of which have found engineering application mainly in investigation of the diffusiophoresis target efficiency for an evaporating or condensing drop [**Placek and Peters**, 1980].

2. Formulation of the problem

Let us consider two pervious spheres of radius 'a' and 'b' (where b >a) with sink of strength '-Q' at its centre generating radial inward flow around it in an infinite expense of incompressible fluid of density ρ and kinematic viscosity ν. The spheres are also made to rotate with small steady angular velocities Ω_1 and Ω_2 so that terms of an $o(\Omega^2)$ may be neglected but terms of $o(Q\Omega)$ retained. The motion of this formulation has been taken from the author's previous works [**Datta and Srivastava**, 2000, **Srivastava et al.**, 2011] due to the fact that body geometry has not been changed, although the two concentric spheres are rotating slowly with different angular velocities instead of only one. The governed equations of motion will remain the same and provide the new solutions under the defined boundary conditions. The main aim of the present formulation is to study the effect of sink at the centre of slowly rotating spheres over torque to maintain the motion.

The motion is governed by steady Navier-Stokes equations

$$\mathbf{u}\ .grad\,\mathbf{u} = -\left(\frac{1}{\rho}\right) grad\ p\ + \nu\,\nabla^2\mathbf{u} \tag{1}$$

and continuity equation

$$div\mathbf{u}\ = 0, \tag{2}$$

together with no-slip boundary condition

$$\mathbf{u}\ = a\Omega\hat{\mathbf{e}}_x \times \hat{\mathbf{e}}_r, \quad \text{on the inner sphere } r = a, \tag{3a}$$

$$\mathbf{u} = b\Omega\hat{\mathbf{e}}_x \times \hat{\mathbf{e}}_r, \quad \text{on the outer sphere } r = b, \tag{3b}$$

and the condition of vanishing of velocity at far-off points

$$\mathbf{u} = 0 \quad \text{as} \quad r \to \infty. \tag{4}$$

The velocity considered in (2.3) is not posed for complete flow, but only for the difference between full velocity and the velocity induced by the sink at centre. In the above equations, symbols $\mathbf{u}$, p , ρ , ν stands for velocity , pressure, density and kinematic viscosity and unit vectors $\hat{\mathbf{e}}_x$ and $\hat{\mathbf{e}}_r$ are along x-axis and radial direction. It will be convenient to work in spherical polar coordinates (r, θ, ϕ) with x-axis as the polar axis. We non-dimensionalize the space variables by a , velocity by a Ω , and pressure by $\rho\,\nu\,\Omega$. Moreover, the symmetry of the problem and the boundary conditions ensure that velocity components $v_r = v_\theta = 0$, and then we may express the non-dimensional velocity vector $\mathbf{u}$ as

$$\mathbf{u} = -\frac{Q}{a^2 r^2}\hat{e}_r + v_\varphi\,(r\,,\,\theta)\,\hat{e}_\varphi \tag{5}$$

and pressure as

$$p = \rho\nu\Omega[p_0(r) + p_1(r,\theta)]. \tag{6}$$

By introducing the expressions (5) and (6) in equation (1), the azimuthal component v_ϕ is seen to satisfy the equation

$$\nabla^2 v_\varphi - \frac{v_\varphi}{r^2\,sin\,\theta} = -\frac{s}{r^3}\frac{\partial}{\partial r}\left(r\,v_\varphi\right), \tag{7}$$

where $s = \dfrac{Q}{\nu\,a}$ is the sink parameter.

The above equation is to be solved under the boundary conditions

$$\left.\begin{array}{l} v_\varphi = \sin\theta \quad \text{at} \quad r = 1\ (\text{non} - \text{dimensional equation of spheres}) \\ \text{and} \\ v_\varphi \to 0 \quad \text{as} \quad r \to \infty. \end{array}\right\} \tag{8}$$

3. Solution

We take the trial solution as

$$v_\phi = r\omega(r)sin\theta, \tag{9}$$

substituting this value of v_ϕ into equation (7), we get, after some calculation and adjustment

$$\frac{d}{dr}\left[r^4\frac{d\omega}{dr} + s\,r^2\omega\right] = 0, \tag{10}$$

and the boundary conditions (8) in non-dimensional form become

$$\omega = 1 \quad \text{at} \quad \text{r} = 1(\text{i.e. on the surface}) \tag{11}$$

and

$$\omega \to 0 \quad \text{as} \quad \text{r} \to \infty. \tag{12}$$

The above boundary conditions may also be express in dimensional form as

$$\omega = \Omega_1 \quad \text{at} \quad \text{r} = \text{a}(\text{i.e. on the inner sphere}) \tag{13}$$

and

$$\omega \to 0 as r \to \infty. \tag{14}$$

On integration of equation (10), we get the solution in non-dimensional form as

$$\omega(r) = \frac{A}{s^3}\left[\frac{s^3}{r^2} + 2\frac{s}{r} + 2\right] + B\, e^{\frac{s}{r}} \tag{15}$$

and in dimensional form as

$$\omega(r) = \frac{A}{s^3}\left[\frac{s^2a^2}{r^2} + 2\frac{sa}{r} + 2\right] + B\, e^{\frac{sa}{r}}, \tag{16}$$

where A and B are constants of integration which can be obtained by applying boundary conditions (13) and (14) as

$$\frac{A}{s^3} = \Omega_1\left[s^2 + 2s + 2 - 2e^s\right]^{-1}$$

and

$$B = -2\Omega_1\left[s^2 + 2s + 2 - 2e^s\right]^{-1}.$$

Substituting the values of constants A and B in (16), we get the expression of angular velocity ω(r) in dimensional form as

$$\omega(r) = \frac{A}{s^3}\left[\frac{s^2a^2}{r^2} + 2\frac{sa}{r} + 2\right] + B\, e^{\frac{sa}{r}}$$

or

$$\omega(r) = \Omega_1\left[\frac{s^2a^2}{r^2} + 2\frac{sa}{r} + 2 - e^{\frac{sa}{r}}\right]\left[s^2 + 2s + 2 - 2e^s\right]^{-1} \tag{17}$$

and consequently, with the help of (9), the expression for azimuthal component of velocity v_ϕ comes out to be in dimensional form as

$$v_\varphi = r\omega(r)\sin\theta = \Omega_1 r\,\sin\theta\left[\frac{s^2a^2}{r^2} + 2\frac{sa}{r} + 2 - e^{\frac{sa}{r}}\right]\left[s^2 + 2s + 2 - 2e^s\right]^{-1}. \tag{18}$$

4. Torque on inner sphere rotating with uniform angular velocity Ω_1 (when outer sphere is also rotating with different uniform angular velocity Ω_2)

If there exists an external concentric pervious sphere of radius b (b>a), rotating with small angular velocity Ω_2 i.e., the boundary conditions for this situation will be

$$\omega = \Omega_2 \quad \text{at} \quad \text{r = b (at outer surface)} \tag{19}$$

and

$$\omega = \Omega_1 \quad \text{at} \quad \text{r = a (at inner surface).} \tag{20}$$

by using the above boundary conditions, in equation (16), the constant of integration A and B comes out to be

$$-\frac{A}{s^3} = \frac{\Omega_1 - \Omega_2 e^{s\left(1-\frac{a}{b}\right)}}{\left[\left(\frac{s^2a^2}{b^2} + 2\frac{sa}{b} + 2\right) e^{s\left(1-\frac{a}{b}\right)} + \left(-s^2 - 2s - 2\right)\right]} \tag{21}$$

and

$$B = e^{-\frac{sa}{b}} \left[\frac{\Omega_1 \left\{\frac{s^2a^2}{b^2} + 2\frac{sa}{b} + 2\right\} + \Omega_2 \left\{-s^2 - 2s - 2\right\}}{e^{s\left(1-\frac{a}{b}\right)} \left\{\frac{s^2a^2}{b^2} + 2\frac{sa}{b} + 2\right\} + \left\{-s^2 - 2s - 2\right\}}\right]. \tag{22}$$

The expression of angular velocity ω(r) can be written with the help of equation (16)

$$\omega(r) = \frac{A}{s^3}\left[\frac{s^2a^2}{r^2} + 2\frac{sa}{r} + 2\right] + B\, e^{\frac{sa}{r}},$$

where A and B are given in (21) and (22). On differentiating the function ω(r), we have

$$\frac{d\omega}{dr} = \frac{A}{s^3}\left[-\frac{2s^2a^2}{r^3} - \frac{2sa}{r^2}\right] + B\, e^{\frac{sa}{r}}\left(-\frac{sa}{r^2}\right) \quad ,$$

the value of $\frac{d\omega}{dr}$ at r = a can be written as

$$\left(\frac{d\omega}{dr}\right)_{r=a} = \frac{1}{a}\left[-\frac{2A}{s^3}\left(s^2 - s\right) - Bs\, e^s\right]. \tag{23}$$

The moment of force p_ϕ is p_ϕ. r sin θ, where $p_\phi = \mu$. r sin θ. $\frac{d\omega}{dr}$, is the only non-vanishing component of force p . If N is the torque on the sphere of radius a, then by using (23), we have

$$N = \int_0^\pi \left(p_\varphi . r \sin\theta\right)_{r=a} dS$$

$$= \int_0^{\pi} \left(\mu r \sin\theta \frac{d\omega}{dr} r \sin\theta \right)_{r=a} . (2\pi a \sin\theta . a\, d\theta)$$

$$= \frac{8}{3}\pi a^3 \mu \left[-\frac{2A}{s^3}\left(s^2 + s\right) + Be^s \right]$$

$$= \frac{8}{3}\pi a^3 \mu \left[\begin{array}{l} 2\left(s^2+s\right)\left\{\Omega_1 - \Omega_2 s e^{s\left(1-\frac{a}{b}\right)}\right\} \\ +se^{s\left(1-\frac{a}{b}\right)}\left\{-\Omega_1\left(\frac{s^2a^2}{b^2}+2\frac{sa}{b}+2\right)+\Omega_2\left(s^2+2s+2\right)\right\} \end{array} \right] \times \left[\left\{ -e^{s\left(1-\frac{a}{b}\right)}\left(\frac{s^2a^2}{b^2}+2\frac{sa}{b}+2\right)+\left(s^2+2s+2\right)\right\}\right]^{-1}. \quad (24)$$

If inner and outer spheres are rotating with same angular velocities, i.e. $\Omega_1 = \Omega_2 = \Omega$ and b = 2a, then from (24), torque coefficient (normalizing with $8\pi\mu a^3\Omega$, torque on sphere having radius 'a') is given by

$$\frac{N}{8\pi\mu a^3\Omega} = \frac{1}{3}\left[8\left(s+s^2\right) - s^2 e^{\frac{s}{2}}(4+5s)\right]\left[4\left(2+2s+s^2\right) - \left(s^2+4s+8\right)e^{\frac{s}{2}}\right]^{-1} \quad (24a)$$

If inner and outer spheres are rotating with different angular velocities, i.e. $\Omega_2 = 2\Omega_1$ and b = 2a, then from (24), torque coefficient (normalizing with $8\pi\mu a^3\Omega_1$, torque on sphere having radius 'a') is given by

$$\frac{N}{8\pi\mu a^3\Omega_1} = \frac{1}{3}\left[8s\left(1+s+e^{\frac{s}{2}}\right) - s^2 e^{\frac{s}{2}}(4+9s)\right]\left[4\left(2+2s+s^2\right) - \left(8+4s+s^2\right)e^{\frac{s}{2}}\right]^{-1} \quad (24b)$$

The rate of dissipated energy is given by $N\Omega_1$, where the value of N is given in equation (24), (24a, b).

5. Torque on outer sphere rotating with uniform angular velocity Ω_2 (when inner sphere is fixed, i.e. Ω_1 =0)

The expression for angular velocity ω(r) is given by (16)

$$\omega(r) = \frac{A}{s^3}\left[\frac{s^2a^2}{r^2}+2\frac{sa}{r}+2\right] + B\, e^{\frac{sa}{r}}.$$

Now we use the following boundary conditions

$$\omega(r) = \Omega_2 \quad \text{on surface} \quad r = b \quad (25)$$

and

$$\omega(r) \to 0 \quad \text{as} \quad r \to \infty. \quad (26)$$

Under these boundary conditions, the values of constant A and B can be obtained as follows

$$\frac{A}{s^3} = \Omega_2 \left[\frac{s^2 a^2}{b^2} + \frac{2sa}{b} - 2e^{\frac{sa}{b}} + 2 \right]^{-1} \tag{27}$$

and

$$B = -2\Omega_2 \left[\frac{s^2 a^2}{b^2} + \frac{2sa}{b} - 2e^{\frac{sa}{b}} + 2 \right]^{-1}. \tag{28}$$

Now, the expression for derivative of angular velocity at r = b comes out to be

$$\left[\frac{d}{dr} \omega(r) \right]_{r=b} = \left[\frac{A}{s^3} \left(-\frac{2s^2 a^2}{r^3} - \frac{2sa}{r^2} \right) + B \left(-\frac{sa}{r^2} \right) e^{\frac{sa}{r}} \right]_{r=b}$$

$$= -\frac{1}{b} \left[\frac{2A}{s^3} \left(\frac{s^2 a^2}{b^2} + \frac{sa}{b} \right) + B \frac{sa}{b} e^{\frac{sa}{b}} \right],$$

which reduces in final form by (27) and (28)

$$= -\frac{2\Omega_2}{b} \left[\frac{s^2 a^2}{b^2} + \frac{sa}{b} - \frac{as}{b} e^{\frac{sa}{b}} \right] \left[\frac{s^2 a^2}{b^2} - \frac{2sa}{b} - 2e^{\frac{sa}{b}} + 2 \right]^{-1}. \tag{29}$$

Hence, torque N on the outer sphere in the presence of inner sphere

$$N = \int_0^{\pi} \left(\mu \,.\, r \,\sin\theta \,.\, \frac{d\omega}{dr} \,.\, r \,\sin\theta \right)_{r=b} (2\pi b \,\sin\theta \,.\, b \, d\theta)$$

$$= \frac{8}{3} \pi \, b^3 \mu \left(\frac{d}{dr} \omega(r) \right)_{r=b},$$

by using (29), it reduces to

$$= \frac{16}{3} \pi \, b^3 \mu \, \Omega_2 \left[\frac{s^2 a^2}{b^2} + \frac{sa}{b} - \frac{sa}{b} e^{\frac{sa}{b}} \right] \left[\frac{s^2 a^2}{b^2} + 2\frac{sa}{b} - 2e^{\frac{sa}{b}} + 2 \right]^{-1}. \tag{30}$$

If b = 2a, then from (30), torque coefficient (normalizing with $8\pi\mu a^3\Omega_2$, torque on sphere having radius 'a') is given by

$$\frac{N}{8\pi\mu a^3 \Omega_2} = \frac{2}{3} \left[2s + s^2 - 2se^{\frac{s}{2}} \right] \left[s^2 + 4s + 8 - 8e^{\frac{s}{2}} \right]^{-1} \tag{31}$$

The expression for rate of dissipated energy will be $N\Omega_2$, where N is given in equation (30) and (31).

6. Particular Cases

Case 1. We consider the outer spherical surface to be fixed i.e., $\Omega_2 = 0$, then in this case, by (24), we have, torque on the inner sphere rotating with angular velocity Ω_1 as

$$N = \frac{8}{3}\pi a^3 \mu \Omega_1 \left[2\left(s^2+s\right) - s\left(\frac{s^2a^2}{b^2} + 2\frac{sa}{b} + 2\right)e^{s\left(1-\frac{a}{b}\right)}\right] \left[\left(-s^2-2s-2\right) + \left(\frac{s^2a^2}{b^2} + 2\frac{sa}{b} + 2\right)e^{s\left(1-\frac{a}{b}\right)}\right]^{-1}. \tag{32a}$$

If b = 2a, then from (32a), torque coefficient (normalizing with $8\pi\mu a^3\Omega_1$, torque on sphere having radius 'a') is given by

$$\frac{N}{8\pi\mu a^3\Omega_1} = \frac{1}{3}\left[8\left(s+s^2\right) - s\left(s^2+4s+8\right)e^{\frac{s}{2}}\right] \left[-4\left(2+2s+s^2\right) + \left(8+4s+s^2\right)e^{\frac{s}{2}}\right]^{-1} \tag{32b}$$

Now, on shifting the solid outer spherical body having radius b (b>a) to infinity i.e., b$\to \infty$, then $e^{s\left(1-\frac{a}{b}\right)} \to e^s$ and by (32a), we can have the expression for torque on slowly rotating inner sphere of radius 'a' alone and given by (32b) as

$$N = \frac{16}{3}\pi\mu a^3\Omega_1 \frac{\left[s^2+s-se^s\right]}{\left[s^2+2s+2-2e^s\right]}, \tag{33}$$

which match with the expression of torque obtained by **Srivastava et al.** [2011] for slowly rotating pervious sphere of radius 'a' rotating with slow uniform angular velocity Ω_1 with sink at the centre and further reduces to classical one $8\pi\mu a^3\Omega_1$ for s = 0 (i.e. in the absence of sink at the center).

Case 2. If the inner sphere rotates with uniform angular velocity Ω_1, while outer rotates with uniform angular velocity Ω_2 at infinity, i.e. b $\to \infty$, then by expression (24), we have the torque on inner sphere as

$$N = \frac{8}{3}\pi\mu a^3 \frac{\left[2\Omega_1\left(s^2+s-se^s\right) + \Omega_2 se^s\left(2-s^2\right)\right]}{\left[s^2+2s+2-2e^s\right]}. \tag{34a}$$

If $\Omega_2 = 2\Omega_1$, then from (34a), torque coefficient (normalizing with $8\pi\mu a^3\Omega_1$, torque on sphere having radius 'a') is given by

$$\frac{N}{8\pi\mu a^3\Omega_1} = \frac{2}{3}\left[s+s^2+se^s\left(1-s^2\right)\right]\left[2+2s+s^2-2e^s\right]^{-1} \tag{34b}$$

If inner and outer spheres are rotating with same angular velocities, i.e. $\Omega_1 = \Omega_2 = \Omega$ and then from (34a), torque coefficient (normalizing with $8\pi\mu a^3\Omega$, torque on sphere having radius 'a') is given by

$$\frac{N}{8\pi\mu a^3\Omega} = \frac{1}{3}\left[2s + 2s^2 - s^3e^s\right]\left[2 + 2s + s^2 - 2e^s\right]^{-1} \tag{34c}$$

Case 3. If we consider the limiting situation as a $\rightarrow$ b and $\Omega_1 \rightarrow \Omega_2$, then we have the expression for torque on slowly rotating sphere having radius 'a' by (30)

$$N = \frac{16}{3}\pi a^3 \mu \Omega_2 \left[s^2 + s - se^s\right]\left[s^2 + 2s + 2 - 2e^s\right]^{-1}, \tag{35}$$

which agrees with that given in the paper of **Srivastava et al.** [2011] and further reduces to the classical one $M_0 = 8\pi\mu a^3\Omega_1$ for s = 0 (i.e. in the absence of sink at the center).

7. Numerical Discussion

Variation of angular velocity ω(r) [equation (17)] with respect to 'r' for various values of sink parameter 's' are shown in Figure 1. For increasing values of 'r' , the value of angular velocity ω(r) gets dampened steadily and reduces ultimately to zero for specific values of sink parameter 's'. It is interesting to note here that for values of 'r' ($0 \leq r \leq 1$), ω(r) sharply comes down to 1, and then slowly dies down to zero for values of r >1. Torque coefficient [equation (24a) and (24b)] for inner rotating sphere decreases with respect to increasing values of sink parameter 's' in the presence of outer sphere having radius 2a and rotating with same angular velocity in first case and $2\Omega_1$ in the second case. Both these variations are depicted in Figures 2 (i) and 2 (ii). Torque coefficient [equation (31)] on outer rotating sphere (in the presence of fixed inner wall) having radius 2a increases from 1 (for s=0) to ∞ with respect to increasing values of sink parameter 's'. Torque coefficient [equation (32b)] on inner wall (in the presence of fixed outer wall having radius 2a) increases from 1.2 (for s=0) to ∞ with respect to increasing values of sink parameter 's'. Further, torque coefficient [equation (34b)] for inner sphere (when outer wall is present at far distance and rotating with angular velocity $2\Omega_1$) increases with respect to increasing values of sink parameter 's'. These variations are depicted in Figures 3, 4 and 5. In all calculations of torque coefficient in different situations, normalization is done via classical value of torque, $8\pi\mu a^3\Omega$, on rotating sphere having radius 'a'.

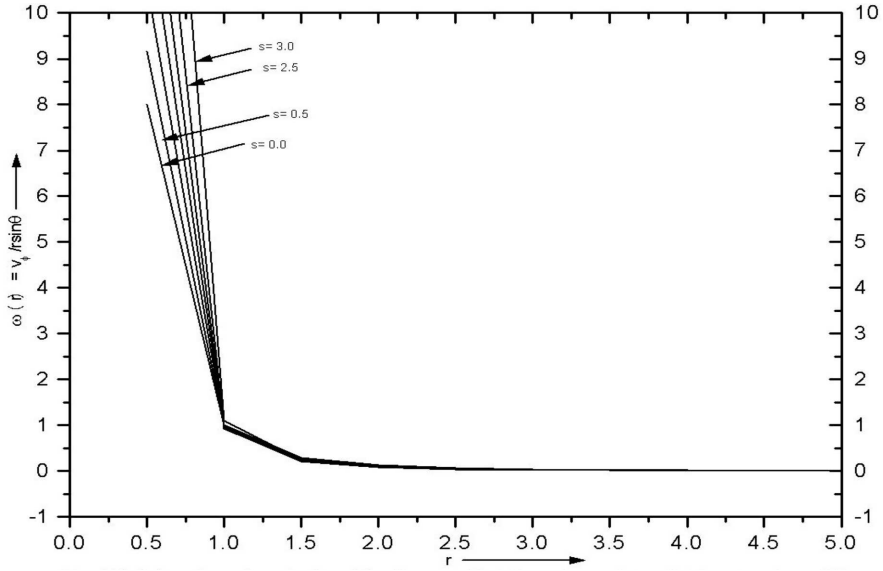

Fig. 1. Variation of angular velocity ω(r) with respect to 'r' for various values of sink parameter s=Q/νa

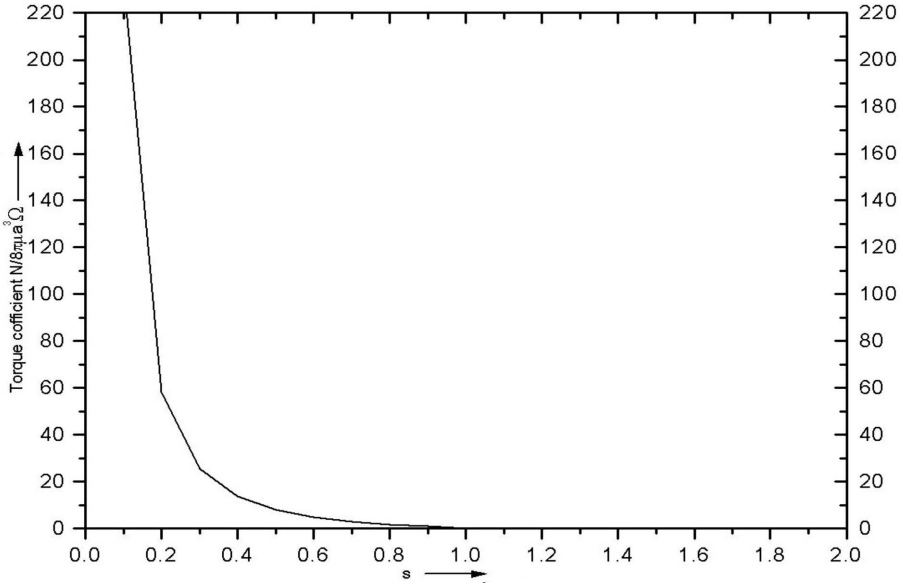

Fig. 2. (i) Variation of Torque cofficient $N/8\pi\mu a^3\Omega$ with respect to sink parameter 's'

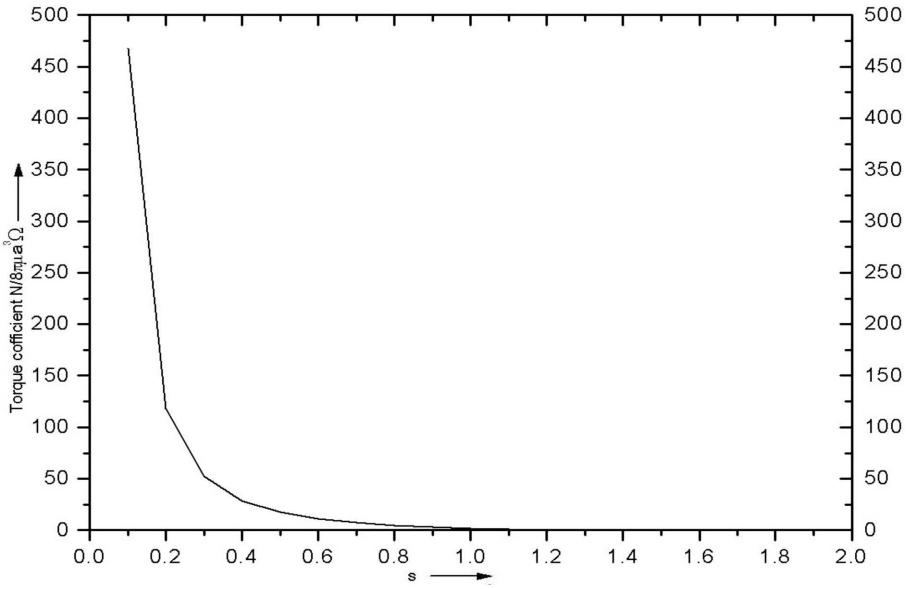

Fig. 2 (ii) Variation of Torque cofficient $N/8\pi\mu a^3\Omega$ with respect to sink parameter 's'

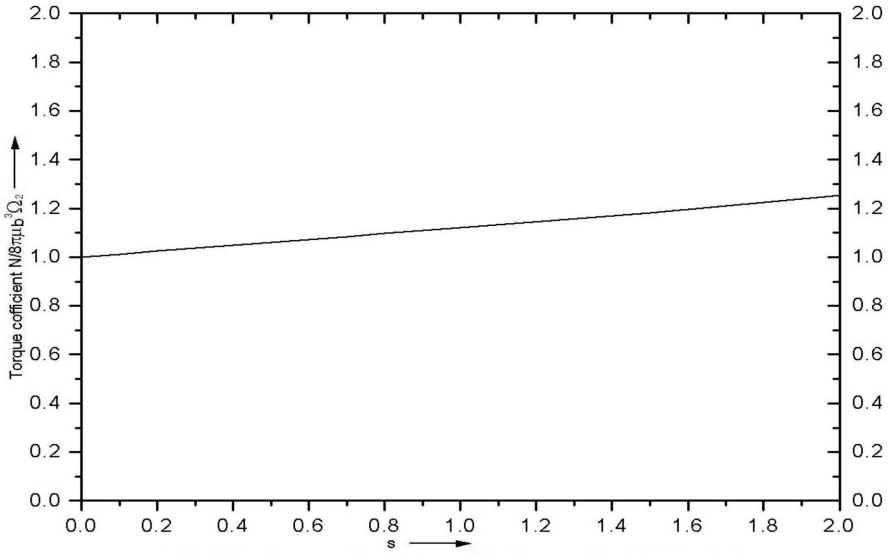

Fig. 3. Variation of Torque cofficient $N/8\pi\mu b^3\Omega_2$ with respect to sink parameter 's'

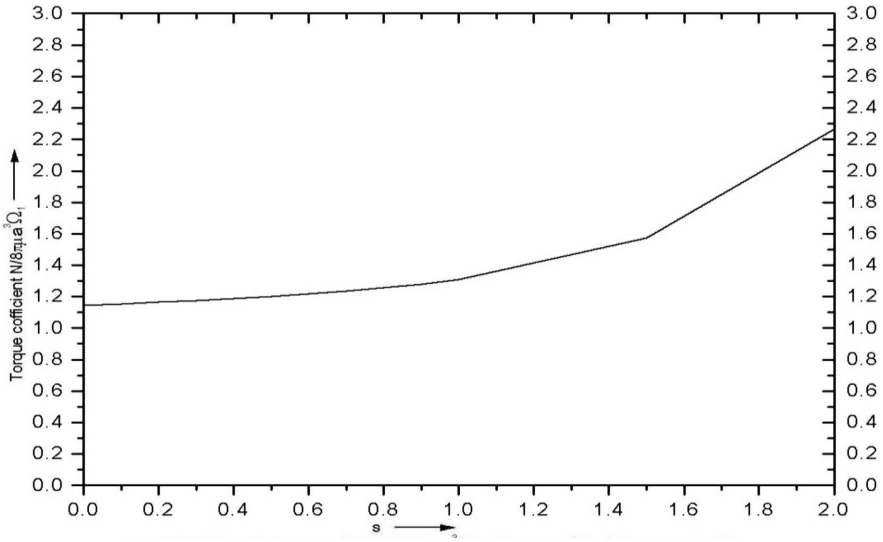

Fig. 4. Variation of Torque cofficient $N/8\pi\mu a^3\Omega_1$ with respect to sink parameter 's'

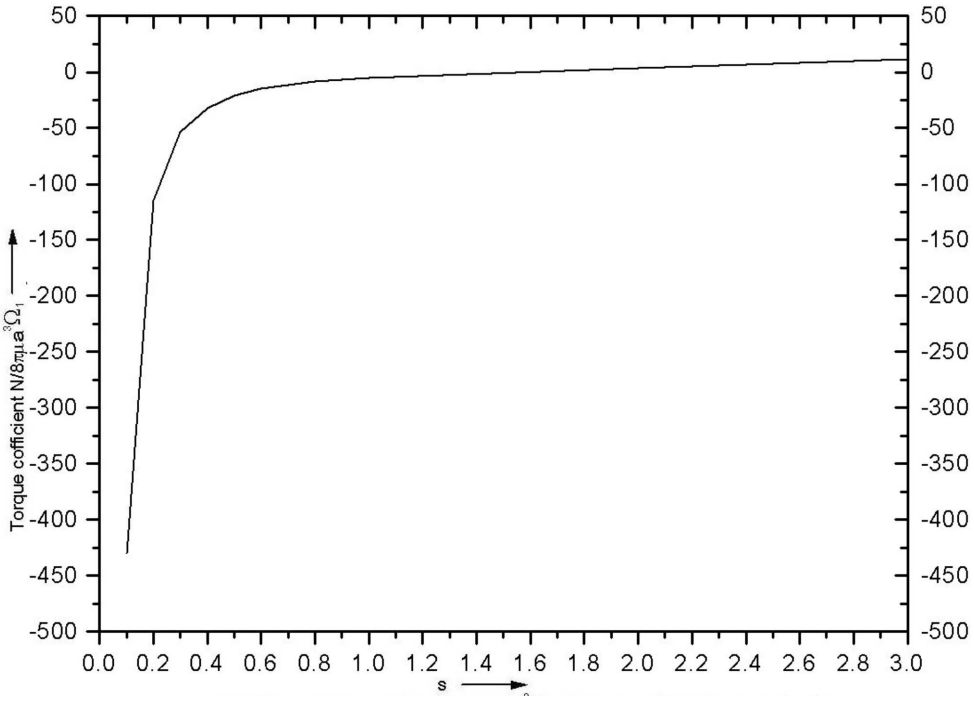

Fig. 5. Variation of Torque cofficient $N/8\pi\mu a^3\Omega_1$ with respect to sink parameter 's'

8. Conclusion

The problem of slow rotation of two concentric pervious spheres having fluid sink at the centre in viscous fluid is solved. The expressions for torque in general case (3.16, 3.22) and in cases (4.1 to 4.3) are calculated and expected to be new and never seen in the literature. It has been observed that rotation of either wall create interference for the rotation of other wall resulting in a decrease of torque with respect to increasing sink parameter. While, on the other hand, torque on either wall increases with respect to increasing values of sink parameter when the other wall is kept fixed. The results found here may be very useful in the study of evaporating or condensing spherical drop in nature.

Acknowledgement

I acknowledge my sincere thanks to the anonymous referees for their invaluable comments and suggestions to improve the quality of the manuscript. I also express my thanks and gratitude to the authorities of B.S.N.V. Post Graduate College, Lucknow (Uttar Pradesh), India, for providing the basic infra structure facilities throughout the preparation of this work at the department of mathematics. Third author (SY) is thankful to University Grants Commission, New Delhi, to provide Junior Research Fellowship.

Manuscript received by Editorial Board, January 23, 2012;
final version, January 02, 2013.

REFERENCES

[1] Barett K. E.: On the impulsively started rotating sphere, Journal of Fluid Mechanics, Vol. 27, 1967, pp. 779.
[2] Brenner H.: The slow motion of a sphere through a viscous fluid towards a plane surface, Chem. Eng. Sci., 16, 1961, pp. 242-251.
[3] Childress S.: The slow motion of a sphere in a rotating viscous fluid, J. Fluid Mech., vol. 20, 1964, pp. 305-314.
[4] Cooley M. D. A.: The slow rotation in a viscous fluid of a sphere close to another fixed sphere about a diameter perpendicular to the line of centers. Quart. J. Mech. Appl. Math. Vol. 24, 1971, pp. 237-250.
[5] Datta S.: Stokes flow past a sphere with a source at its center. Mathematik Vesnik Vol. 10 (25), 1973, pp. 227-229.
[6] Datta S., and Srivastava D. K.: Slow rotation of a sphere in a viscous flow with source at its center. Proc. (Math. Sci.), Indian Academy of Sciences Vol. 110, No. 1, Feb. 2000, pp. 117-120.
[7] Davis A.M.J., and Brenner H.: Steady rotation of a tethered sphere at small, non-zero Reynolds and Taylor numbers: wake interference effects on drag, J. Fluid Mech., vol. 168, 1986, pp. 151-167.

[8] Davis A.M.J.: Force and torque on a rotating sphere close to and within a fluid-filled rotating sphere, American Physical Society, 59^{th} Annual Meeting of the APS Division of Fluid Dynamics, Nov. 19-21, 2006.
[9] Davis M. H.: The slow rotation and translation of two unequal spheres in a viscous fluid. Chem. Eng. Sci. Vol.24, issue 12, Dec. 1969, pp. 1769-1776.
[10] Dennis S. C. R., Ingham D.B., and Singh S.N.: The steady flow of a viscous fluid due to a rotating sphere, Quart. J. Mech. Appl. Math., vol. 34, 1981, pp. 361-381.
[11] Drew D.A.: The force on a small sphere in slow viscous flow, J. Fluid Mech., vol. 88, 1978, pp. 393-400.
[12] Gagliardi, John Charles: Analytical studies of axially symmetric motion of an incompressible viscous fluid between two concentric rotating spheres, Ph.D. Thesis, Marquette University, Milwaukee, W.I., 1987.
[13] Gagliardi, John Charles, Nigro N.J., Elkouh A.F., Yang J.K., and Rodriguez L.: Study of the axially symmetric motion of an incompressible viscous fluid between two concentric rotating spheres, J. Engrg. Math., vol. 24, 1990, pp. 1-23.
[14] Happel J., and Brenner H.: Low Reynolds number hydrodynamics, Prentice Hall Englewood, 1965, 1985, Clifs NJ.
[15] Ifidon E. O.: Numerical studies of viscous incompressible flow between two rotating concentric spheres, Journal of Applied Math. (Hindawi Pub.), vol. 2, 2004, pp. 91-106.
[16] Jeffrey G. B.: On the steady rotation of a solid of revolution in a viscous fluid. Proc. Lond. Math. Soc. vol. 14 (1915), pp. 327-338.
[17] Kanwal R.P.: Slow steady rotation of axially symmetric bodies in a viscous fluid. J. Fluid Mech. vol. 10 (1960), pp. 17-24.
[18] Kanwal R. P.: Note on slow rotation or rotary oscillations of axi-symmetric bodies in hydrodynamics and magnetohydrodynamics. J. Fluid Mach. vol. 41, no. 4, 1970, pp. 721-726.
[19] Karanfilian S.K., and Kotas T.J.: Motion of a spherical particle in a liquid rotating as a solid body, Proc. Roy. Soc. London Ser. A, vol. 376, 1981, pp. 525-544.
[20] Kim Dong Joo, and Choi Hae Cheon: Laminar flow past a sphere rotating in the streamwise direction. J. Fluid Mech. vol. 461, 2002, pp. 365-386.
[21] Kim Moon-Uhn: Slow viscous rotation of a sphere on the axis of a circular cone. Physics of Fluid, Vol. 23, issue 6, 1980, pp. 1268-1269.
[22] Kohr Mirella, and Pop I.: Incompressible Flow for Low Reynolds Numbers, W.I.T. Press, Southampton, U.K., 2004.
[23] Lamb H.: Hydrodynamics. Dover Publications, 1954.
[24] Landau L.D., and Lifshitz E.M.: (1959, 1976, 1984) Fluid Mechanics, Pergamon Press, New York., 1959, 1976, 1984.
[25] Langlois L.E.: Slow Viscous Flow, Macmillan Publishers, NY, USA, 1964.
[26] Liu M., Delgado A., and Rath H.J.: A numerical method for study of the unsteady viscous flow between two concentric rotating spheres, Computational Mechanics, vol. 15, no. 1, 2004, pp. 45-57.
[27] Majumdar S.R.: On the slow motion of viscous liquid in space between two eccentric spheres, J. Phys. Soc. Japan, vol. 26, no. 3, 1969, pp. 827.
[28] Marcello Romano: Exact analytic solutions for the rotation of an axially symmetric rigid body subjected to a constant torque, Celestial Mechanics and Dynamical Astronomy, vol. 101, no. 4, 2008, pp. 375-390.
[29] Marcus Philips S., and Tuckerman Laurette S.: Simulation of flow between concentric rotating spheres. Part 1. Steady Case, J. Fluid Mech., vol. 185, 1987, pp. 1-30. [Part 2, Transitions, J. Fluid Mech., vol. 185, 1987, pp. 31-65].
[30] Munson B.R., and Joseph D.D.: Viscous incompressible flow between concentric rotating spheres. Part 1. Basic flow, J. Fluid Mech., vol. 49, 1971, pp. 289-318. [Part2. Hydrodynamic stability, J. Fluid Mech., vol. 49, no. 2, 1971, pp. 305-318].

[31] Munson B.R., and Menguturk M.: Viscous incompressible flow between concentric rotating spheres. Part 3. Linear stability and experiments, J. Fluid Mech., vol. 69, 1975, pp. 705-719.
[32] O'Neill M.E., and Majumdar R.: Asymmetrical viscous fluid motions caused by the translation or rotation of two spheres. Part 1: The determination of exact solutions for any values of the ratio of radii and separation parameters, Z.A.M.P., vol. 21, no. 2, 1970, pp. 164-179.
[33] O'Neill M.E., and Majumdar R.: Asymmetrical viscous fluid motions caused by the translation or rotation of two spheres. Part 2: Asymptotic forms of the solutions when the minimum clearance between the spheres approaches zero, Z.A.M.P., vol. 21, no. 2, 1970, pp. 180-187.
[34] O' Neill M.E., and Yano H.: The slow rotation of a sphere straddling a free surface with a surfactant layer. Quart. J. Mech. Appl. Math. vol. 41, 1988, pp. 479-501.
[35] O' Neill M.E., Ranger K. B., Brenner H.: Slip at the surface of a free surface bounding a semi-infinite viscous fluid: Removal of the contact-line singularity. Physics of Fluid, vol. 29, no. 4 (1986), pp. 913-924.
[36] Placek Timothy D., and Peters Leonard K.: A hydrodynamic approach to particle target efficiency in the presence of diffusiophoresis. J. Aerosal Sci. vol. 11 (1980), pp.521-533.
[37] Pearson Carl E.: A numerical study of the time dependent viscous flow between two rotating spheres. J. Fluid Mech. vol. 28, 1967, p.323.
[38] Philander S. G. H.: On the flow properties of a fluid between concentric spheres. J. Fluid Mech. vol. 47, no. 4, 1971, pp.799.
[39] Pozrikidis C.: Introduction to theoretical and computational fluid dynamics, Oxford University Press, 1997.
[40] Proudman I.: The almost rigid rotations of viscous fluid between concentric spheres, J. Fluid Mech., vol. 1, 1956, pp. 505-516.
[41] Ranger K. B.: Time dependent decay of the motion of a sphere translating and rotating in a viscous liquid. Quart. J. Mech. Appl. Math. vol. 49, no. 4, 1996, pp. 621-633.
[42] Ranger K. B.: Slow viscous flow past a rotating sphere. Proc. Camb. Phil. Soc. vol.69 (1971), p.333.
[43] Riley T.: Thermal effects on slow viscous flow between rotating concentric spheres, International J. Non-Linear Mechanics, vol. 7, no. 3, 1972, pp. 275-288.
[44] Rubinow S.I., and Keller J. B.: Transverse force on a spinning sphere moving in a viscous fluid, J. Fluid Mech., vol. 11, 1961, pp. 447-459.
[45] Srivastava D.K., Yadav R.R., and Yadav Supriya: Slow rotation of sphere with sink at the centre of sphere in a viscous fluid, Proc. National Symposium on Application of Various Techniques in Fluid Dynamics, 2011, pp. 217-224. [**ISBN:9788192132303**].
[46] Stewartson K.: On almost rigid rotations: Part 2., J. Fluid Mech., vol. 26, 1966, pp. 131-144.
[47] Singh S.N.: The flow past a spinning sphere in a slowly rotating fluid at small Reynolds number, Intl. J. Engrg. Sci., vol. 13, 1975, pp. 1085-1089.
[48] Takagi Hideaki: Slow rotation of two touching spheres in a viscous fluid, J. Phys. Soc. Japan, vol. 36, no. 3, 1974, pp. 875.
[49] Takagi Hideaki: On the slow motion of a sphere in a viscous fluid, J. Phys. Soc. Japan, vol. 37, no. 2, 1974, pp. 505.
[50] Takagi Hideaki: Viscous flow induced by slow rotation of a sphere, J. Phys. Soc. Japan, vol. 42, no. 1, 1977, pp. 319.
[51] Tekasakul P., Tompson R.V., and Loyalka S.K.: Rotatory oscillations of arbitrary axi-symmetric bodies in an axi-symmetric viscous flow: Numerical solutions, Physics of Fluids, vol. 10, no. 11, 1998, pp. 2797-2818.
[52] Tekasakul P., and Loyalka S.K.: Rotatory oscillations of axi-symmetric bodies in an axi-symmetric viscous flow with slip: Numerical solutions for spheres and spheroids, Int. J. Num. Meth. Fluids, vol. 41, no. 8, 2003, pp. 823-940.
[53] Wakiya Shoichi: Slow motions of a viscous fluid around two spheres, J. Phys. Soc. Japan, vol. 22, no. 4, 1967, pp. 1101.

[54] Wimmer Manfred: Experiments on a viscous fluid flow between concentric rotating spheres, J. Fluid Mech., vol. 78, 1976, pp. 317-335.

[55] Yang Jen-Kang, Nigro Nicholas J., Elkouh Andel F., and Gagliardi John Charles: Numerical study of the axially symmetric motion of an incompressible viscous fluid in an annulus between two concentric rotating spheres, Int. J. for Numerical Methods in Fluids, vol. 9, no. 6, 1989, pp. 689-712.

Przepływ stokesowski wokół powolnie wirujących koncentrycznych kul przepuszczalnych

S t r e s z c z e n i e

W artykule rozważa się problem koncentrycznych kul przepuszczalnych, ze zlewem płynu w centrum, które wirują powoli wokół średnicy z jednostajnymi prędkościami kątowymi Ω_1 i Ω_2. Analiza wykazała, że istnieje tylko azymutalny składnik prędkości, a moment obrotowy i szybkość rozpraszania energii są w istniejących warunkach wyznaczane analitycznie. Wyprowadzono wyrażenie na moment obrotowy na powierzchni wewnętrznej kuli powolnie wirującej z jednostajną prędkością kątową Ω_1, podczas gdy kula zewnętrzna także powolnie wiruje z jednostajną prędkością kątową Ω_2. Zbadano także przypadki szczególne, takie jak: (i) kula wewnętrzna jest nieruchoma (tzn. $\Omega_1 = 0$), podczas gdy kula zewnętrzna wiruje z jednostajną prędkością kątową Ω_2, (ii) kula zewnętrzna jest nieruchoma (tzn. $\Omega_2 = 0$), podczas gdy kula wewnętrzna wiruje z jednostajną prędkością kątową Ω_1, (iii) kula wewnętrzna wiruje z jednostajną prędkością kątową Ω_1, podczas gdy kula zewnętrzna wiruje w nieskończonej odległości z prędkością kątową Ω_2. Na wykresach przedstawiono zależności między zmianami momentu obrotowego a parametrami zlewu.

THE ARCHIVE OF MECHANICAL ENGINEERING

VOL. LX 2013 Number 2

10.2478/meceng-2013-0012

Key words: Shell Eco-Marathon, fuel economy

PAWEŁ SULIKOWSKI [*], *RYSZARD MAROŃSKI* [**]

QUASI-PERIODIC CONTROL TECHNIQUE FOR MINIMIZING FUEL CONSUMPTION DURING RECORD VEHICLE COMPETITION

The problem of the optimal driving technique during the fuel economy competition is reconsidered. The vehicle is regarded as a particle moving on a trace with a variable slope angle. The fuel consumption is minimized as the vehicle covers the given distance in a given time. It is assumed that the run consists of two recurrent phases: acceleration with a full available engine power and coasting down with the engine turned off. The most fuel-efficient technique for shifting gears during acceleration is found. The decision variables are: the vehicle velocities at which the gears should be shifted, on the one hand, and the vehicle velocities when the engine should be turned on and off, on the other hand. For the data of students' vehicle representing the Faculty of Power and Aeronautical Engineering it has been found that such driving strategy is more effective in comparison with a constant speed strategy with the engine partly throttled, as well as a strategy resulting from optimal control theory when the engine is still active.

1. Introduction

Modern motor companies design new cars mostly taking into account relatively small operation costs. Such tendencies are enforced by competition on the market. Also the fuel companies, including Royal Dutch Shell, propagate technologies reducing the fuel consumption by cars. The new ecological technologies are tested during different events, including the annual competition called the Shell Eco-Marathon. Its aim is to encourage young enthusiasts to design vehicles minimizing the fuel consumption. The competition is divided into two categories: the prototype vehicles and the urban cars. Each category is divided into classes with respect to the engine used

[*] *Student of Faculty of Power and Aeronautical Engineering, Warsaw University of Technology; E-mail: paw.sulikowski@gmail.com*

[**] *Institute of Aeronautics and Applied Mechanics, Warsaw University of Technology; E-mail: maron@meil.pw.edu.pl*

(piston engine or electrical one) and the fuel (gasoline, ethanol, gas, oil). The Students' Vehicle Aerodynamics Association affiliated at the Faculty of Power and Aeronautical Engineering, Warsaw University of Technology, participates in the category of prototype vehicles powered by gasoline piston engines.

The success in this competition depends on two elements. The first one is the optimal construction of the minimal mass vehicle, generating minimal aerodynamic and rolling losses, using a high efficient engine. The second element is the strategy employed during the competition. This also may be optimized. The following paper is devoted to that second element.

In the paper by Rogowski and Maroński (2009) the problem of the optimal driving strategy during the fuel economy competition is considered. The vehicle is regarded as a particle moving on the trace with a variable slope angle. This version of the vehicle is not equipped with a gear-box (the transmission ratio is constant). The velocity is controlled by the power setting. The problem is formulated in the optimal control approach and solved using a direct pseudospectral Chebyshev's method (Fahroo and Ross, 2002). This approach, despite being correct from the methodological point of view, gives the result worse than that obtained during the real event in 2006, Nogaro, France. Therefore, the minimum-fuel problem is reconsidered using the assumptions better adjusted to the real competition, the data for the current version of the students' vehicle and the data for the new trace in Lausitz, Germany.

2. Problem formulation

Fundamental assumptions of the mathematical model are as follows (cf. Rogowski and Maroński, 2009):

1. The record vehicle is regarded as a particle.
2. The motion takes place in the vertical plane. The shape of the trace is described by a given smooth function h(x) of the horizontal coordinate x.
3. The vehicle is equipped with a gear-box, therefore the optimal shifting strategy should be computed. This is the first fundamental difference in comparison with the paper by Rogowski and Maroński (2009).
4. The brakes are not used.
5. The velocity of the vehicle is quasi-periodically controlled via turning on and off the engine. When the engine is running it generates its maximal power (no engine throttling). The vehicle velocities when the engine should be turned on and off are not known. This is the second fundamen-

tal difference in comparison with the paper by Rogowski and Maroński (2009).

6. The wind and any other random factors, like the existence of another competitors, are not considered.
7. The mass of the vehicle is constant. The amount of the fuel consumed is insignificant in comparison with the total mass of the vehicle. This assumption is not valid in the aircraft dynamics (Panasz and Maroński, 2005).
8. The local slope of the trace β is small, therefore $\cos\beta \approx 1$.
9. The indicators on the dashboard show: the vehicle velocity, the rotational speed of the engine, the covered distance and the time from the start. Basing on these parameters, the optimal strategy should be realized by the driver during the event.

Assumption 5 needs an explanation. In the paper by Rogowski and Maroński (2009), the optimal result is about 37% worse in comparison with the result obtained during real competition in Nogaro, France, 2006. It is due to the assumption that the engine is constantly active during the run and the velocity is controlled via throttling the engine power. The diagram of the specific fuel consumption versus rotational speed and power setting shows that the specific fuel consumption takes minimal value close to the maximal power setting and it is relatively high for minimal power setting (cf. Fig. 3 in Rogowski and Maroński, 2009). It gave us the impulse for further analysis of the problem.

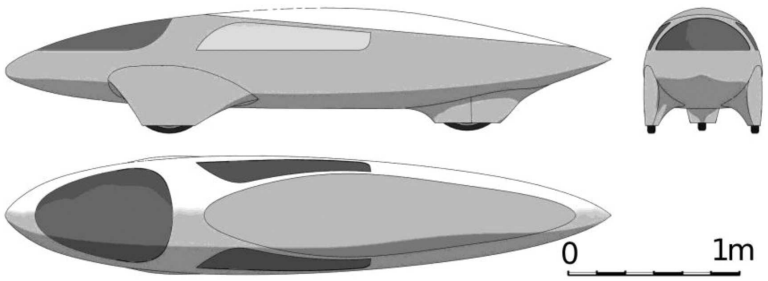

	symbol	value	unit
vehicle's mass	m_0	46	kg
driver's mass	m_k	64	kg
frontal area	A	0,3743	m^2
wheel diameter	-	0,479	m

Fig. 1. Students' record vehicle "Droplet" ("Kropelka" in Polish) and its geometrical and mass data

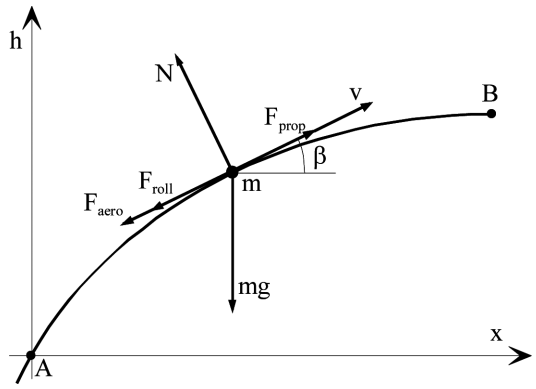

Fig. 2. Particle model of the record vehicle. The forces exerted on the vehicle are: F_{aero} – aerodynamic drag, F_{roll} – rolling resistance, F_{prop} – forward propulsive force, N - normal reaction of the ground, mg - weight. A and B are initial and final points respectively, h(x) is the shape function of the trace, x is the horizontal coordinate (approximately covered distance), m is the mass of the vehicle with the driver, v is the velocity of the vehicle, β is the local slope of the trace

The equations of vehicle motion resulting from the second Newton law are as follows (cf. Arczyński, 1994; Maroński, 1999; Maroński, 2002; Rogowski and Maroński, 2009)

$$m \frac{dv}{dt} = F_{prop} - F_{aero} - F_{roll} - F_g, \tag{1}$$

$$\frac{dx}{dt} = v \cos\beta \approx v, \tag{2}$$

where:

$$F_g = m\, g \sin\beta, \tag{3}$$

$$F_{roll} = N\, C_{roll} = m\, g \cos\beta\, C_{roll} \approx m\, g\, C_{roll} = \text{const}., \tag{4}$$

$$F_{aero} = 0.5\, \rho\, A\, C_D\, v^2, \tag{5}$$

$$F_{prop} = \frac{M\,[\omega\,(v,u)]\;\;\omega\,(v,u)\;\;\eta\,(u)}{v}. \tag{6}$$

The symbols used are: t – time, F_g – gravitational force component onto direction of motion, g – gravitational acceleration, C_{roll} – rolling resistance coefficient, ρ - air density, A – frontal projection area, C_D – drag coefficient, M – torque, ω – engine rotational speed, u – transmission ratio, η – efficiency.

The propulsive force F_{prop} is computed from equation (6) if both of the following conditions are satisfied:

– the engine is turned on,
– the rotational speed of the engine is greater than its minimal value ω_{MIN} =209.3 rad/s (2000 rev/min).

If the first condition is satisfied but the second is not, the clutch is activated. It happens especially at the start to the event. Further details one can find in Sulikowski (2011).

The boundary conditions represent the vehicle velocities at the beginning and at the end of the race:

$$v(t_A) = v_A = 0, \quad v(t_B) = v_B = v_{FINISH} . \tag{7}$$

Minimized is the total amount of fuel G_p used to cover the given distance from A to B

$$G_p = \int_A^B sfc(v,u)\, M(v,u)\, \omega(v,u)\, \eta(u)\, dt , \tag{8}$$

where sfc is the specific fuel consumption. The integrand in (8) attains zero as the engine is not active.

From the regulations of the competition it follows that the average velocity v_{AV} should be no less than 30 km/h, $v_{AV} \geq 30$ km/h. According to equation (5), the aerodynamic drag rapidly increases with a velocity, therefore in the presented reasoning the inequality constraint is replaced by the equality constraint

$$v_{AV} = \frac{L}{t_B - t_A} = 30\, km/h = 8.33\, m/s, \tag{9}$$

where L is the total length of the trace [m].

The goal of the analysis is minimization of the overall fuel consumption during Shell-Eco Marathon represented by the integral (8). The conditions (1)-(7) and (9) should be satisfied. Due to assumption 5, the vehicle control function is quasi-periodic. It means that the distance is divided into sections. Each of them contains two phases: the active phase (acceleration), where the engine propels the vehicle with a maximal power setting, and the passive phase (deceleration) when the vehicle coasts down. The switching velocities, the maximal v_{MAX} and the minimal one v_{MIN}, during the phases are the same in the whole race and they should be computed. During the first phase (acceleration), the shifting strategy minimizing the fuel consumption should be found. The switching points also depend on the vehicle velocity and this can be easily observed and remembered by the driver. The shifting strategy remains the same in further part of the trace, regardless of the local slope of terrain.

3. Data of the record vehicle

The basic geometrical data of students' vehicle "Droplet" are taken from an existing construction – the current version of the vehicle. The mass data are derived from the protocol after the technical inspection during the event, in May 2010. The frontal projection area is obtained by integrating the area of the vehicle shadow during projection on the plane perpendicular to the direction of motion. Fig. 1 contains these geometrical and mass data.

The estimation of the rolling resistance F_{roll} and the dependence of the velocity on aerodynamic drag (eq. 5) is of primary importance. The share of the aerodynamic and rolling losses is different for a record vehicle in comparison with the classical car (Piechna, 2000), therefore the rolling and aerodynamic resistances have been measured during the series of experiments conducted by the Students' Vehicle Aerodynamics Association. For this study it is assumed that the data from a free coasting down give the better results in comparison with towing. Finally, the rolling resistance is F_{roll} =4.22 N and the drag coefficient is C_D =0.1373. Further details referring to the experiments and the method of estimation one can find in Sulikowski (2011).

The students' record vehicle is powered by the petrol piston engine Honda GX25, having a capacity of 25 cm^3. For the standard regulations of this engine and the maximal power setting, the specific fuel consumption versus rotational speed is given in Fig. 3a. Fig. 3b illustrates the maximal power and the maximal torque versus rotational speed (Honda engines, 2010).

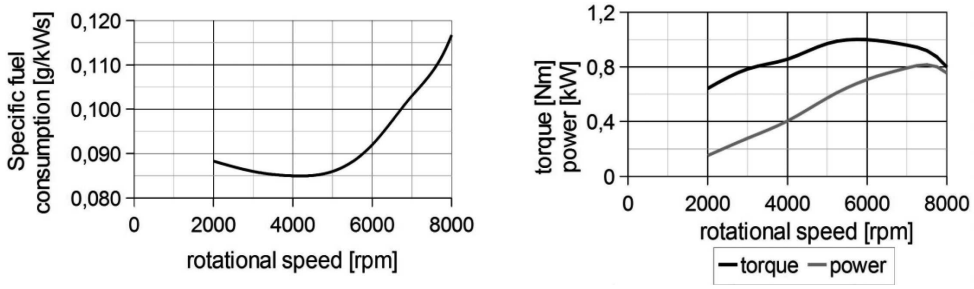

Fig. 3. Engine specific fuel consumption versus its rotational speed, and maximum available engine power and torque versus its rotational speed

The shape of the trace in Lausitz, Germany (elevation of the terrain above horizontal versus distance) is depicted in Fig. 4 (grey line). This figure shows a profile of one lap. During the competition the vehicles cover 8 laps.

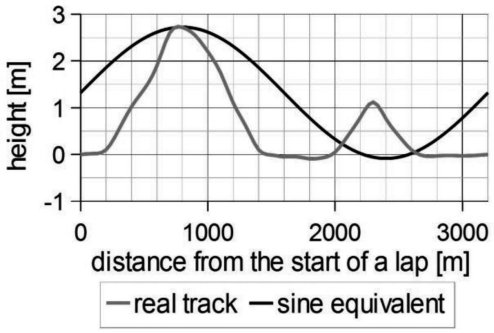

Fig. 4. Shape of the trace (one lap)

4. Optimal shifting strategy

The record vehicle is equipped with two reducers and a gear-box. The first reducer decreases the rotational speed of the engine. Its ratio is constant and equal to u=1.8. Further, the torque is transmitted to the rear wheel hub via the chain transmission, whose ratio is u=7.0. The gear-box within the hub has 14 gears. The ratios and efficiencies for different gears are depicted in Fig. 5 and computed basing on producer's data (Rohloff, 2010).

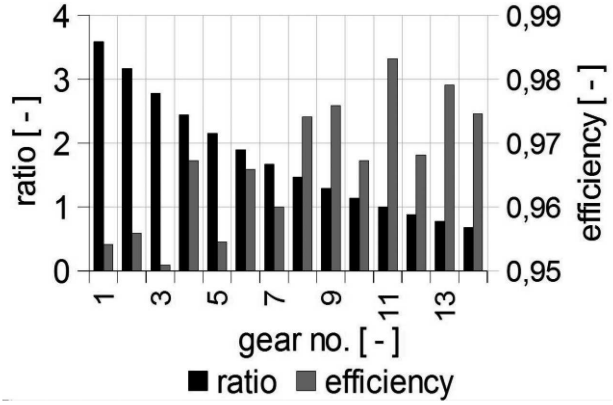

Fig. 5. Ratios and efficiency at different gears

Summing up, the driver may select the actual ratio from a range of 8.316 to 45.108.

The optimization is put into practice under the following assumptions:

- Only one cycle is considered when the vehicle accelerates with maximal power of the engine up to the maximal velocity equal to 15 m/s (this limitation follows from the safety conditions). The vehicle moves on the flat sector of the trace.

- From the construction of the gear-box it follows that shifting the gears is done one by one (any gear cannot be omitted).
- The amount of fuel consumed during acceleration is minimized. Optimized is the number of the gear (one from fourteen) and the vehicle velocity when this gear should be shifted up.

The genetic algorithm, called the simulated annealing, is used for the solution of this problem. It is employed along with the AB-mutation of the variables. The details one can find in Sulikowski (2011), Kirkpatrick et al. (1983), Grygiel (2000).

Up to the year 2009, the "Droplet" was equipped with a transmission with the constant ratio u=14.5. Application of the gear-box lets the engine operate with the rotational speed close to the minimum of the specific fuel consumption (cf. Fig. 3a). Fig. 6 shows the optimal velocities where the gears should be shifted (black squares). For example, for the velocity 2.13 m/s the gear should be shifted from 1 via 2 and 3 to 4. Omitting the gears number 2 and 3 is not possible for this type of gear-box. The solid black line (near horizontal) shows the specific fuel consumption for the vehicle equipped with gear-box. The solid grey line shows the specific fuel consumption for the previous version of the vehicle with constant transmission ratio u=14.5. Acceleration from 0 to 15 m/s using optimal shifting the gears gives 43% saving in comparison with acceleration using a constant transmission ratio (previous version of the "Droplet").

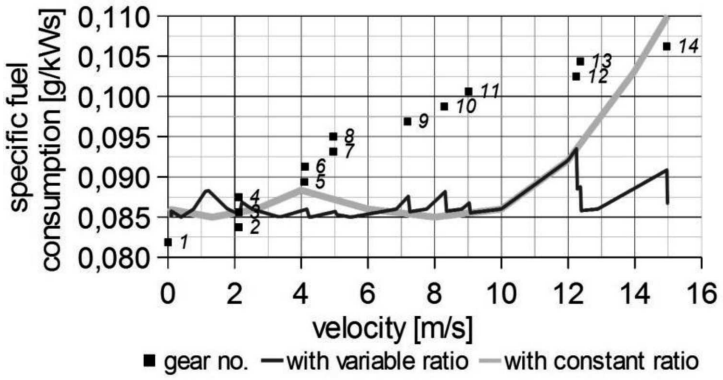

Fig. 6. Optimal shifting the gears from 0 to 15 m/s (black squares). Specific fuel consumption for optimal shifting (black line) and for the constant transmission ratio (grey line)

5. Optimal engine control strategy

Due to assumption 5, the vehicle is powered by the engine that is quasi-periodically turned on and off during the run. The distance may be divided

into sections (not necessary equidistant) where the vehicle accelerates with the maximal engine power setting, and where the vehicle coasts down with the engine turned off. Typically, the engine works with its maximal efficiency for the power setting referring to 80÷90% of maximal power for a given rotational speed. The savings in the specific fuel consumption is about 1÷5% in comparison with a non throttled regime (Edgar, 2008). For the sake of simplicity of the driving technique used during the race, it is much more comfortable to use maximal power than a sophisticated throttle control (Rogowski and Maroński, 2009).

It is known from the literature that the vehicle's velocity at the end of the run should be relatively low. Such an element of the strategy is called "the negative kick" in competitive running (Maroński, 1996). It makes it possible to consume the kinetic energy of the vehicle at the finish. The finish velocity v_{FINISH} is not known, and it should be computed. The other decision variable is the minimal velocity v_{MIN} when the engine is turned on after each phase of free coasting down (the passive, unpowered section). The unknown is also the maximal velocity v_{MAX} where the engine is turned off after each acceleration phase. However, this variable may be computed from the equality constraint v_{AV} =30 km/h.

The problem of the optimal engine control strategy is formulated as follows. Find the vehicle velocities (v_{MIN}, v_{MAX}, v_{FINISH}) minimizing the fuel consumed during the event. The distance to be covered is 25 485 m. The strategy assumes the cycles consisting of accelerations with the maximal engine power and decelerations when the engine is not active, therefore the differential equation of motion (1) should be held in each point of the trace. The optimal shifting strategy described in section 4 is employed during acceleration phases. The vehicle starts with zero velocity and the average velocity during the whole race should be equal to 30 km/h. The formulated problem has been solved using an exhaustive search algorithm.

At the beginning, the assumptions and the method have been verified on an idealized sinusoidal trace similar to Lausitz event track (cf. black line in Fig. 4). Two strategies are compared: a simple constant velocity strategy (v=8.33 m/s), and an optimal quasi-periodic strategy. In both cases, the same distance (25 485 m) has been covered in the same time. Computations indicate that for such simplified trace the optimal fuel consumption is 15.81 g and that is equivalent to the distance to be covered 1134 km using 1 liter of fuel. The constant velocity strategy gives the fuel consumption equal to 28.45 g. Such poor result follows from the relatively high specific fuel consumption for partly throttled regimes which are necessary for keeping the vehicle's velocity constant.

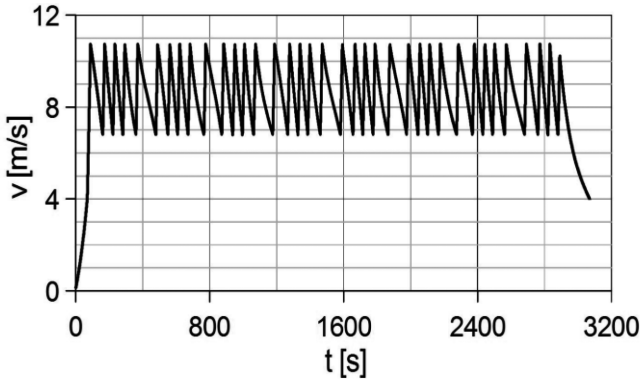

Fig. 7. Optimal vehicle velocity versus time for simplified sinusoidal track

The optimal results for Lausitz event track (grey line in Fig. 4) are depicted in Fig. 8. Here the vehicle accelerates just after the start, then the quasi-periodic strategy is used. The vehicle coasts down at the finish to the velocity v_{FINISH} that is less than v_{MIN}. The disturbances of the periods in the velocity diagram follows from the local slope of terrain that varies with the distance. The engine is turned on 39 times during the record run (excluding the start of the engine at the beginning of the race).

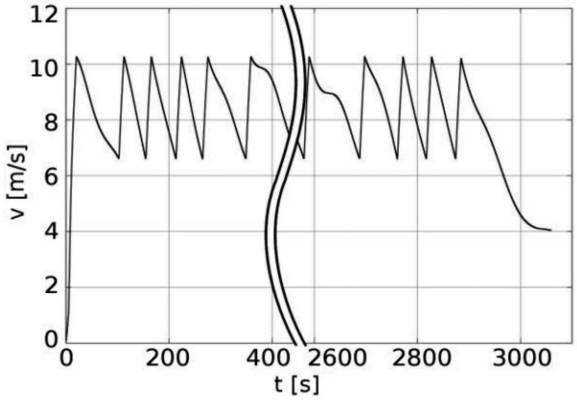

Fig. 8. Optimal vehicle velocity versus time for Lausitz event track

Fig. 9 shows the distance to be covered using 1 liter of the fuel p_2 versus v_{MIN} and v_{FINISH} (v_{MAX} results from the constraint that v_{AV} =30 km/h). It follows from the picture that the optimal result is relatively insensitive to the velocity at the finish v_{FINISH}. It is due to the fact that kinetic energy accumulated in the vehicle's body is relatively small in comparison with the energy necessary for covering the whole distance (more than 25 km).

The quasi-periodic strategy has been compared with the constant velocity strategy. The gear is selected in such a manner that the rotational speed of

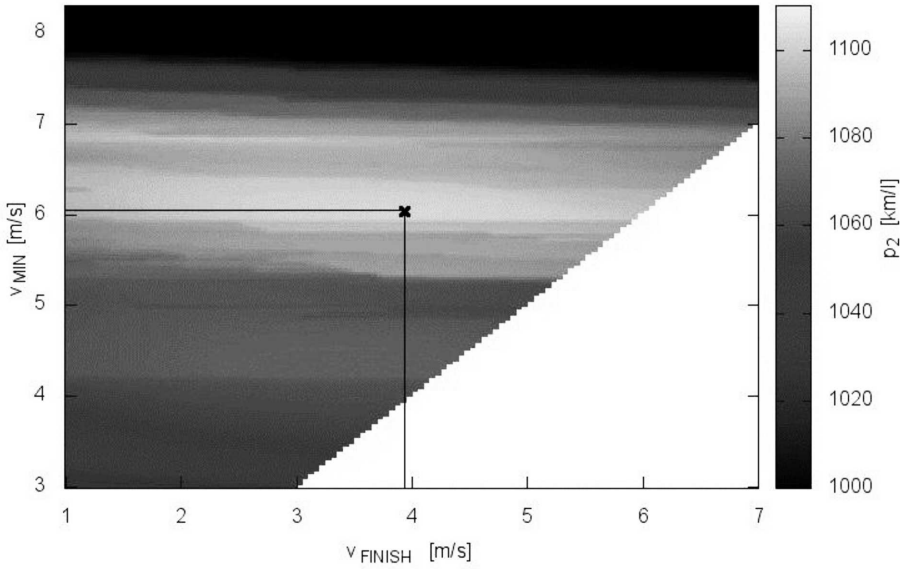

Fig. 9. The distance to be covered using 1 liter of fuel for different v_{MIN} and v_{FINISH}. The cross indicates the optimum

the engine is about 4 000 rev/min. That approximately refers to the minimal specific fuel consumption for the non-throttled regime. The power necessary for vehicle propulsion is about 15% of the maximal power, and it means that the specific fuel consumption is much greater (Edgar, 2008). Computations indicate that such a regime needs about 40% more fuel for covering the same distance with the same average velocity.

The question may arise on the superiority of the quasi-periodic strategy over that resulting from optimal control as far as the fuel consumption is concerned (Rogowski and Maroński, 2009). For comparing both strategies, the quasi-periodic control is computed using vehicle and track data published by Rogowski and Maroński (2009). The transmission ratio is assumed to be constant and the same as the previous one. For such a case, the optimum velocity and the throttle setting are given in Fig. 10. The engine is active only for 20.5% of the total time of the run. Computations indicate that the vehicle is able to cover the distance of 1033 km using 1 liter of fuel, in comparison with 307.4 km/l when using the previous strategy. This example confirms that the quasi-periodic strategy is much better.

6. Conclusions

In this study, the optimal driving strategy during the fuel economy competition is reconsidered. In contrary to the solution by Rogowski and Maroń-

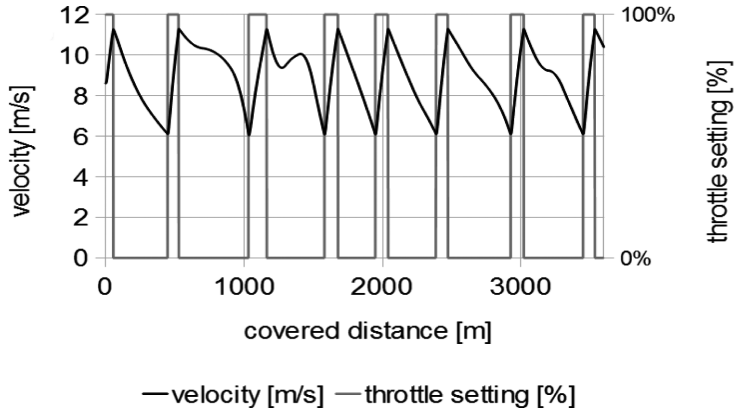

Fig. 10. Optimal velocity and throttle setting versus distance for the quasi-periodic control, and the trace and data published by Rogowski and Maroński (2009)

ski (2009), the quasi-periodic regime is employed. It contains sections where the vehicle accelerates to the maximal velocity v_{MAX} with maximal power setting and then it coasts down to the minimal velocity v_{MIN} where the engine is turned on again. The cycle is repeated as many times as necessary. Shifting the gears is optimized during the acceleration also with respect to the minimum fuel consumption. Comparison of the quasi-periodic strategy with the constant velocity strategy shows about 40% savings of fuel. The quasi-periodic strategy is also significantly fuel-saving in comparison with that one resulting from optimal control (Rogowski and Maroński, 2009). It may be put into practice easily. Here the velocity indications decide how to shift the gear and when the engine should be turned on/off. This is a practical advantage of the quasi-periodic strategy in comparison with a strategy following from an application of the optimal control theory, where the engine should be optimally throttled during the whole race.

Manuscript received by Editorial Board, February 23, 2012;
final version, February 14, 2013.

REFERENCES

[1] Arczyński S.: 1994, *Mechanika ruchu samochodu*, WNT, Warszawa (in Polish).
[2] Edgar J.: 2008, Brake specific fuel consumption, *AutoSpeed*, http://autospeed.com/cms/A_110216/article.html.
[3] Fahroo F., Ross M.: 2002, Direct Trajectory Optimization by a Chebyshev Pseudospectral Method, *Journal of Guidance, Control, and Dynamics*, **25**, 1, 160-166.
[4] Grygiel K.: Warszawa 2000, Algorytmy ewolucyjne z AB-mutacją, Materiały krajowej konferencji „Algorytmy ewolucyjne i optymalizacja globalna" (in Polish).
[5] Honda engines. Technical specifications, active in 2010, http://engines.honda.com/models/model-detail/gx25.

[6] Kirkpatrick S., Gelatt C.D., Vecchi M.P.: 1983, Optimization by simulated annealing, *Science. New Series 220*, nr 4598, 671-680.
[7] Maroński R.: 1999, *Metody rachunku wariacyjnego w biomechanice*, Oficyna Wydawnicza Politechniki Warszawskiej, Warszawa (in Polish).
[8] Maroński R.: 2002, Optimization of cruising velocity in recreational cycling, *Acta of Bioengineering and Biomechanics*, **4**, Suppl. 1, 552-553
[9] Maroński R.: 1996, Minimum-time running and swimming: an optimal control approach, *Journal of Biomechanics*, **29**, 245-249
[10] Panasz P., Maroński R.: 2005, Commercial aircraft trajectory optimization by a Chebyshev's pseudospectral method, *The Archive of Mechanical Engineering*, **LII**, 1, 5-19.
[11] Piechna J.: 2000, *Podstawy aerodynamiki pojazdów*, WKŁ, Warsaw (in Polish).
[12] Rohloff: active in 2010, http://www.rohloff.de/en/technology/speedhub/efficiency_measurement/index.html.
[13] Rogowski K., Maroński R.: 2009, Driving techniques for minimizing fuel consumption during record vehicle competition, *The Archive of Mechanical Engineering*, **LVI**, 1, 26-35.
[14] Sulikowski P.: 2011, *Optimization of the engine regime for the record vehicle minimizing the fuel consumption during the Shell Eco-Marathon competition*, Praca Dyplomowa Inżynierska, Wydział Mechaniczny Energetyki i Lotnictwa Politechniki Warszawskiej (unpublished).

Quasi-okresowa strategia sterowania minimalizująca zużycie paliwa podczas zawodów pojazdów rekordowych

S t r e s z c z e n i e

Rozważono zagadnienie wyznaczenia optymalnej strategii sterowania pojazdem w czasie zawodów pojazdów rekordowych. Pojazd jest modelowany jak punkt materialny poruszający się po trasie o zmiennym kącie pochylenia. Minimalizowana jest ilość zużytego paliwa potrzebna do pokonania zadanego dystansu w zadanym czasie. Opracowano najbardziej efektywną technikę zmiany biegów w czasie przyspieszania. Założono, że pojazd jest napędzany w dwóch trybach: przyspieszania przy pełnej dostępnej mocy silnika i wybiegu, kiedy to silnik jest wyłączony. Zmiennymi decyzyjnymi są: numer biegu oraz prędkość pojazdu, przy której powinno nastąpić jego przełączenie z jednej strony, oraz prędkości pojazdu, przy których silnik powinien być włączony lub wyłączony, z drugiej. Wykorzystując dane pojazdu studentów reprezentujących Wydział Mechaniczny Energetyki i Lotnictwa Politechniki Warszawskiej wykazano, że taka strategia jest bardziej efektywna niż strategia jazdy ze stałą prędkością z częściowym dławieniem silnika oraz pewna strategia wynikająca z teorii sterowania optymalnego, gdzie silnik jest stale włączony.

THE ARCHIVE OF MECHANICAL ENGINEERING

VOL. LX 2013 Number 2

10.2478/meceng-2013-0013

Key words: F-duct, forced separation

PAULINA PIETRZAK, JANUSZ PIECHNA *

NUMERICAL INVESTIGATION OF THE CONTROLLABLE WING STALL CAUSED BY THE AIR INJECTION

This paper presents results of numerical investigation on a controllable airfoil flow separation phenomena practically applied in Formula One racing by a device called the F-duct. Separation is forced by air jets from slots located at different positions on the profile of the dual element wing and is intended to reduce aerodynamic drag. Slot position and the air jet velocity are the main parameters controlling the flow separation. The flow structure, surface pressure distribution, and the generated downwards lift and drag forces were investigated in this study. Two different flow separation structures have been recognised. Typically, wing stall is correlated with an increase in aerodynamic drag force. However, in the case of the finite wing with low aspect ratio, the induced drag is dominant and is proportional to the downforce. Therefore, flow separation on the wing increases the profile drag while simultaneously reducing the induced drag, resulting in a decrease in the total aerodynamic drag.

1. Introduction

Wings are the typical elements used in racing cars for aerodynamic downwards lift generation. The rear wing produces about 35% of the total aerodynamic downforce of a car, which enhances the dynamic handling and stability, although at the same time, it generates 30% of the total aerodynamic drag [1]. As a consequence, a compromise must be found between the maximum cornering speed, which is greatly influenced by the negative lift force, and the reduction of the racing car's top speed due to drag generation.

There are about 20 active Formula One racetracks in the world, each of them requiring specific aerodynamic settings according to the diverse tracks characteristics. For instance, as shown in Figure 1, the Monza course has long straights and fast corners, and therefore requires minimal downforce

* *Warsaw University of Technology, The Faculty of Power and Aeronautical Engineering, 00-665 Warsaw, Nowowiejska 24; E-mail: jpie@meil.pw.edu.pl*

that in turn leads to lower drag and, consequently, higher top speed. On the other hand, Circuit de Monaco, allocated to the city streets, has tight corners which require a high aerodynamic downforce in order to maximise the grip of the tyres. Therefore, in order to avoid prominent aerodynamic drag on the straight section of the racetrack, a very eligible solution would be the use of a movable rear wing.

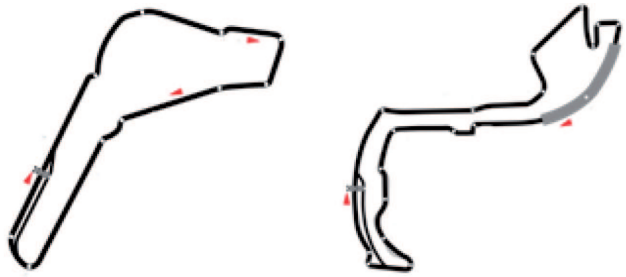

Fig. 1. Autodromo Nazionale Monza and Circuit de Monaco

In the past, the driver from the cockpit controlled the angle of attack of the wing mechanically; it was increased before entering a corner to generate higher downforce, and then reduced on the straight [2]. Two serious accidents that took place during the Grand Prix Barcelona in 1969 resulted in a strong tightening of the FIA regulations. One of the main principles of the rules, applicable right up until the year 2011, was to fix the aerodynamic device geometry, which did not allow changes in the angle of attack to be made during the race.

A racing car is a high-speed prototype, it is constantly evolving, developing, losing weight, gaining speed. The rate of development is so intense that teams introduce a new part to the car on average every 17 minutes [6]. As a consequence, the Formula One regulations are modified frequently, causing permanent discussion between designers and FIA. Engineers, competing to find innovations that match with regulations, try to outdo each other in finding clever ways of evading the rules. Each season, they implement new innovative methods of generating downforce with the purpose of achieving better results. The best ideas are copied by other teams, while the authorities have to control all technical solutions to ensure the safety of teams and spectators in case of an accident. A significant solution development in the 2010 season was the mysterious ‘RW80’ applied in McLaren’s MP4-25 racing car. The inlet to the system was situated under the letter F of the ”Vodafone” branding located at the top of the car body, which is why the system was eventually dubbed the “F-duct” by journalists.

McLaren’s team pioneered a neat solution that allows the driver to control the flow over the rear wing by means of a special duct allocated inside the

racing car. Engineers used the driver's movement as the switch, and since the driver was not considered an aerodynamical device, the system did not infringe the regulations. The air inlet is located in the front part of the racing car in the upper body between the front wheels. The conduit continues along the body, running next to the driver, and ends at an outlet to the rear wing. In the cockpit, there is a vent that is blocked by the driver's left leg, which is not in use on long straights. Consequently, the air which normally comes into the cockpit is redirected to the duct and, with the air from the gearbox, led towards rear wing's slots and disturbs the flow over the wing. Pressure changes caused by the injection of air through small outlets on the rear wing affect the wing in such a way that it enters a stalled state at high speed, reducing aerodynamic drag, and allowing the car as much as an extra 6 mph (9.7 km/h) on straights. Since the F-duct conduit was located inside the body which has been homologated as a whole, other teams could not see the details of this solution.

McLaren used stall to reduce the aerodynamic drag of a rear wing, which naturally occurs when the value of the angle of attack is increased. As shown in Figure 2, at low angles of attack, lift coefficient C_l rises linearly with the angle of attack, and the flow is attached over the entire edge of the profile. A survey of the airfoil aerodynamics indicates that the value of the lift generated is the result of the difference between positive pressure distribution on one side of the wing, and negative pressure distribution on the other [2]. Moreover, Figure 2 shows that the profile drag coefficient C_d increases with the angle of incidence.

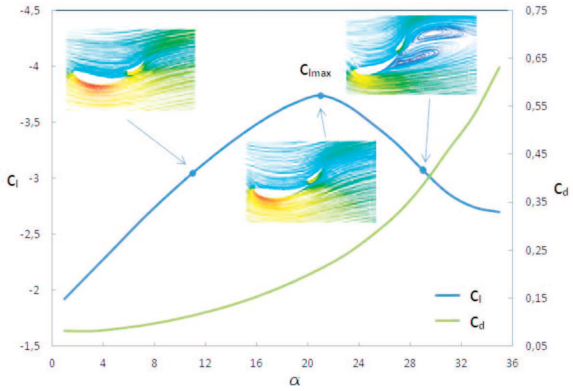

Fig. 2. Variation of lift and drag coefficient with angle of attack

Therefore, as shown in Figure 3, an increase in the angle of attack causes a drop in the pressure value on the lower edge, resulting in a rise in the pressure difference between edges. However, at a certain angle of attack, the downforce coefficient reaches its maximum value C_{lmax} and starts decreasing

due to flow separation on the bottom edge. The wing profile is stalled, and a higher pressure after the point of detachment occurs. Consequently, the wing works effectively only on a part of its surface, and produces less downwards lift. Flow separation creates a wake of turbulent flow behind the wing profile. The velocity in the area of detachment is low, while the pressure at the surface of the wing remains constant, close to ambient pressure.

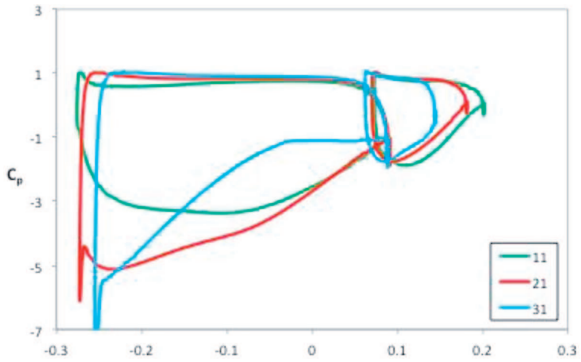

Fig. 3. Surface pressure coefficient distribution over the profile for angles of attack 11, 21 and 31 deg

Increasing the angle of attack raises the value of the profile drag coefficient, as shown in Figure 2. This increase is significant, and is caused by a rise in pressure drag due to flow separation. One may ask why does the stall of a rear wing, which is correlated with an aerodynamic drag force increase, enhance the speed of a race car on straight sections of the race track? The reason is that the aerodynamic drag also consists of the drag linked to the effects of vortices in the flow that form on the wing edges and propagate in the flow behind the wing, as shown in Figure 4.

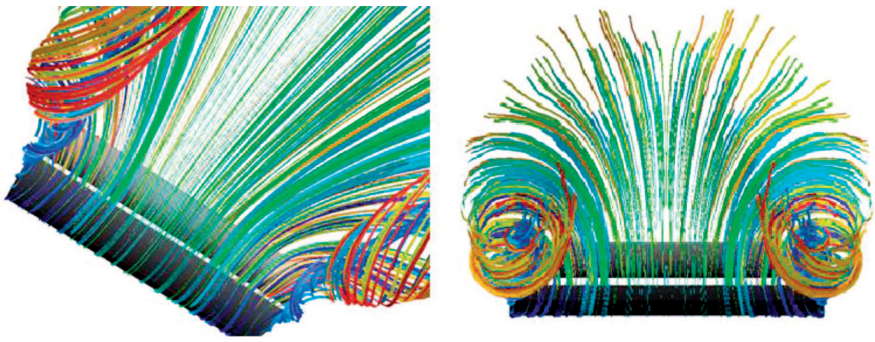

Fig. 4. Propagation of the edge vortices in the flow behind the wing

This is called the induced drag, and is an inevitable consequence of the generation of downforce by means of a finite wing span. The flow over the

wing tends to flow from the high pressure surface towards the low pressure surface, as shown in Figure 5, leaking around the tips of the wing and creating two strong vortices. Edge vortices therefore shed from the wing side edge, changing the velocity and direction of the airflow behind the trailing edge, deflecting it downwards, and thus inducing a downwash behind the wing. The strength of the vortex is directly related to the produced lift. Therefore, the decrease in downforce caused by stall is very important because it reduces the induced drag. The analysis of the flow over the wing in two dimensions assumes that the wing is infinitely long. Therefore, such a study does not include the span dimension of the wing, and thus also does not take into account all the phenomena associated with three-dimensionality of the flow [3,4].

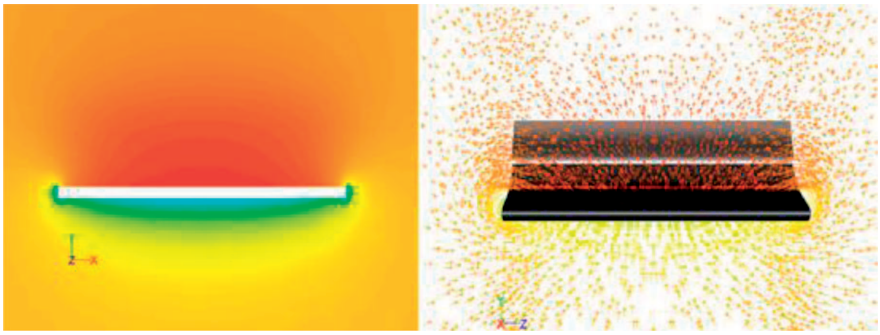

Fig. 5. Computed pressure contours and velocity vectors on the cross section along the wing span

Teams have known for a long time that stalling the rear wing drastically reduces downforce and, as a result, decreases aerodynamic drag. McLaren's engineers obtained stall by forcing separation by altering the flow over the wing via introducing an air stream from slots placed in the lower surface. Similar solutions have already been employed, e.g. flexible wings deflecting due to high speed. However, these have been forbidden after several accidents, and the rear wings became subject to static load tests. McLaren came up with the F-duct idea initially, though there have been other attempts of recreation by Sauber, Williams, and Ferrari with a changing level of success. Some systems developed by manufacturers require the driver to remove a hand from the steering wheel in order to close the vent, which has raised questions about the safety of use. During voting, most teams opted for forbidding the use of the system in the next season.

Any data describing the aerodynamic drag reduction caused by controlled flow separation are not published, so the main aim of the paper is the presentation of results of numerical investigations on these phenomena. The research was based on the position of duct outlets located on the main and secondary profile element, which was a primary geometrical parameter

tested. Moreover, the influence of the slot air stream velocity on the strength of separation, surface pressure distribution, and the generated lift and drag forces was investigated.

2. Simulation of controlled flow separation

Test case description

The geometry employed in the two-dimensional simulation of the controlled flow separation on a two-element wing was the rear wing profile designed for the Formula Student race. It was a dual-element profile consisting of airfoil GOE525 as the main element, and an additional element located to achieve the greatest possible downforce. A numerical simulation was conducted for 5 models with different localisations of the slots introducing air streams in directions normal to the airfoil surface. There were three air outlets on the main profile, and two on the secondary profile element located at the bottom edge in the positions shown in the Figure 6. The profile data were collected for two angles of attack equal to 11° and 21°. To perform the numerical simulation, we employed the software package ANSYS®. The grid was prepared in Gambit ®, and the numerical analysis was conducted using Fluent ®.

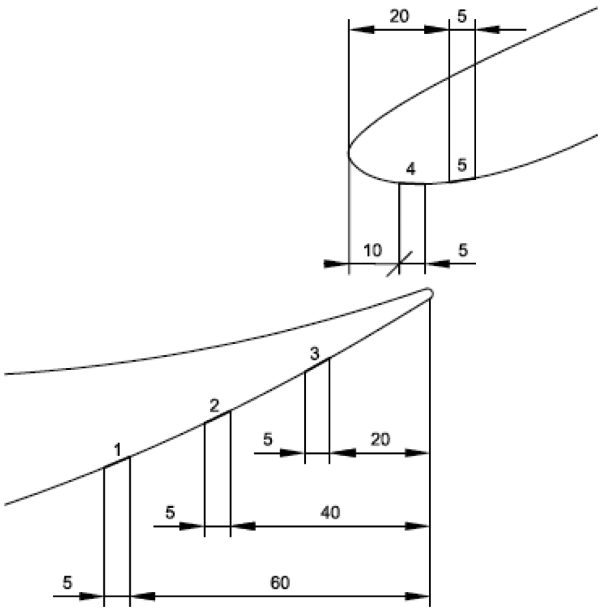

Fig. 6. Location and numbering of slots

3. Computational domain

The computational domain, shown in Figure 7, was created as a rectangular wind tunnel test section, the length and a width of which were 20 m and 10 m, respectively. It was divided into two areas, the inner, which formed a circle with a radius of 1.5 m and the outer, its complement. The centre of the inner surface was located 6 m from the inlet and 1 m from the bottom to take into consideration the additional effects due to ground proximity. The domain consisted of external boundaries: inlet, outlet, bottom, top and internal: interface, profile, and slot.

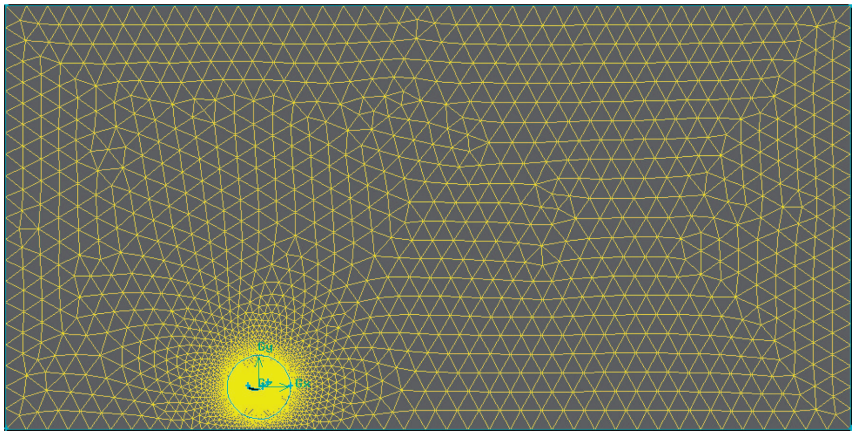

Fig. 7. Computational domain

Nodes were distributed on the profile edges as shown in Figure 8, with their interval decreasing gradually in the direction of leading and trailing edges, and in proximity of the slot. The grid comprised two main parts: the near field, which was formed of triangular elements with a successive expansion ratio 1.05, a maximum height 50 mm evolving in the far field domain with a ratio of 1.25, and 500 mm maximum cell height. The other part, a dense field applied to take into account the changes occurring in the velocity boundary layer, consisted of 15 layers of a rectangular near-wall grid surrounding the profile, as shown in Figure 9.

4. Boundary conditions

Non-slip boundary conditions were applied on the top and bottom profile edges. A constant value of the velocity normal to the boundary was applied on the inlet and in the slots. The pressure outlet boundary condition was applied in the outlet boundary. Numerical analysis was carried out for viscous fluid with Spalart-Allmaras turbulence model [5]. The velocity at the inlet was 30

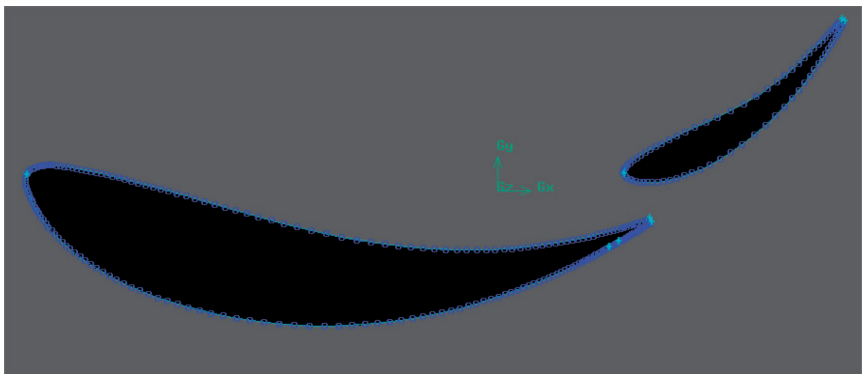

Fig. 8. Nodes distribution on the profile edges

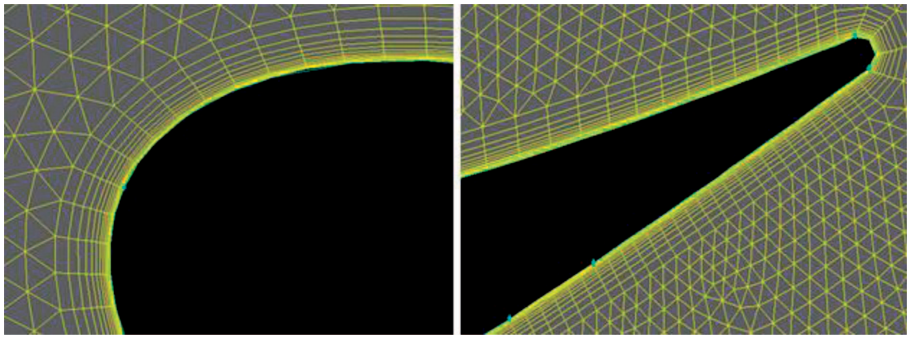

Fig. 9. Distribution of the near-wall layers

m/s, while setting the turbulent intensity and the turbulent length scale to 3% and 0.003 m, respectively. The simulation was conducted for slot velocities of 0, 5, 10, 15, 20, 25, and 30 m/s.

5. Results of numerical simulations

In order to understand how the F-duct system works, the analysis and discussion of the results was divided into two parts. First, the value of the lift and drag coefficient, which varied with the velocity of the injected air stream at the outlet of the duct, was discussed based on the pressure distribution. Second, the value of induced drag was estimated, and the total drag coefficient was analysed with taking into account the influence of the additional air streams provided to flow. Additionally, the relation of the induced and profile drag was included. The aim of this research was to provide a numerical analysis of the introduction of a disturbance to the flow over the wing, which forces a controlled separation, and induces stall. The position of slots was the primary geometrical parameter investigated.

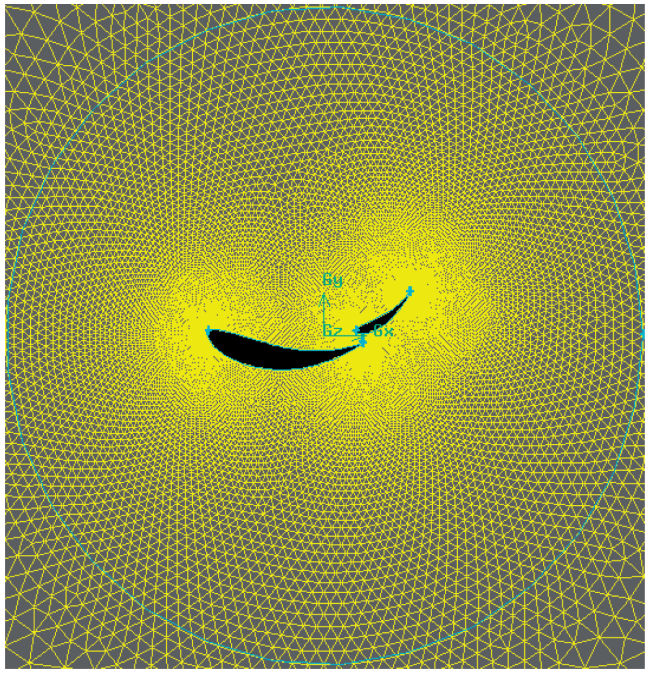

Fig. 10. Cells distribution in the near filed

6. Lift and drag coefficient

Figures 11-14 show the variation of the lift and profile drag coefficient versus slot air velocity for 5 models obtained for angles of attack equal to 11° and 21°. The air jets velocity was expressed in relation to the free stream velocity over the wing profile. The collated results show that, with an increase in the velocity, a significant decrease in the value of the lift coefficient is observed. Additionally, with a growth in duct outlet velocity, one can notice a rise in profile drag coefficient.

The value of the lift coefficient for outlets located on the main profile at an 11° angle of attack decreased gradually, maintaining a generally linear character. However, for the 21° angle of attack at which the maximum lift coefficient was obtained, an increase in velocity at the slot located at the main wing resulted in a drop in the value of the lift coefficient, and that dependence was nonlinear. This was caused by the natural occurrence of flow separation forced by setting the airfoil at the angle of attack for which C_{lmax} was obtained.

For 11° angle of incidence, as shown in Figure 16, there occurred velocity separation beginning from the lowest air stream slot, and with increasing flow velocity in the air stream slot the area of detachment extended and increased its intensity. Flow separation created a wake of turbulent flow behind the wing

profile. Figure 15 shows the pressure distribution over the profile at 11° angle of attack and for slot 1 activated. It can be noticed that the pressure on the lower edge of the main element increased with an increase in outlet velocity from the duct. Moreover, downstream of the air injection, the pressure grew with the slot air velocity until it reached a value close to the ambient pressure and remained constant. All this meant that the wing profile was stalled and consequently the higher pressure after the point of detachment caused an increase in pressure on the lower surface similar to the natural separation that would occur due to the increasing angle of attack. As a result, the wing worked effectively only on a part of its surface and produced less negative lift force. The pressure coefficient distribution plots also show clearly that the pressure around an additional element did not change with the variation of velocity in slots located at the main profile. Therefore, the introduction of the air stream had no effect on the flow around an additional element profile to which the flow remained attached.

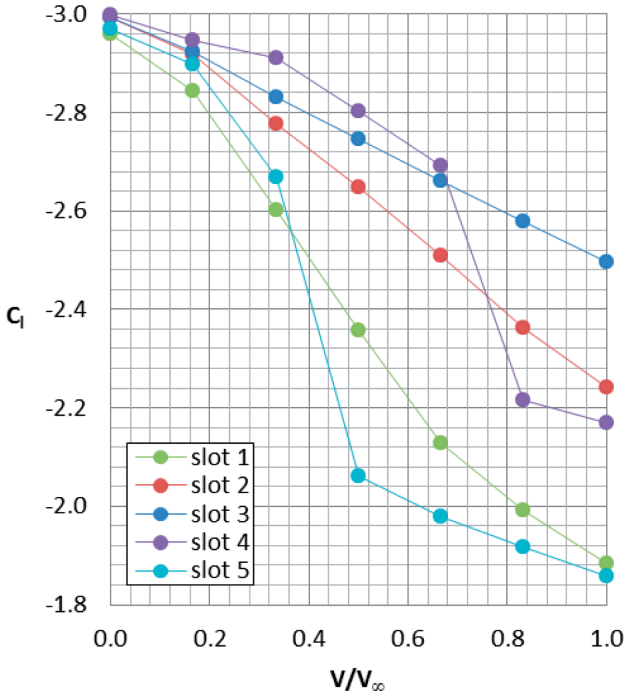

Fig. 11. Calculated lift coefficient at 11° of incidence

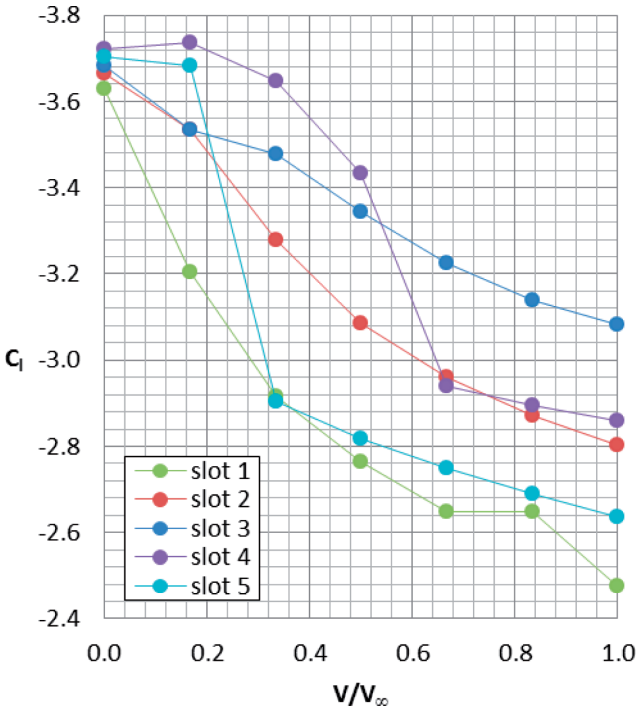

Fig. 12. Calculated lift coefficient at 21° of incidence

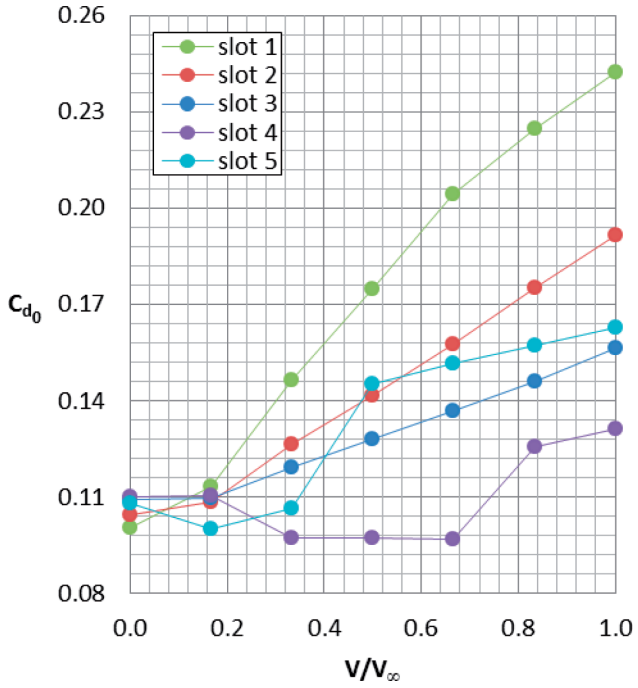

Fig. 13. Calculated drag coefficient at 11° of incidence

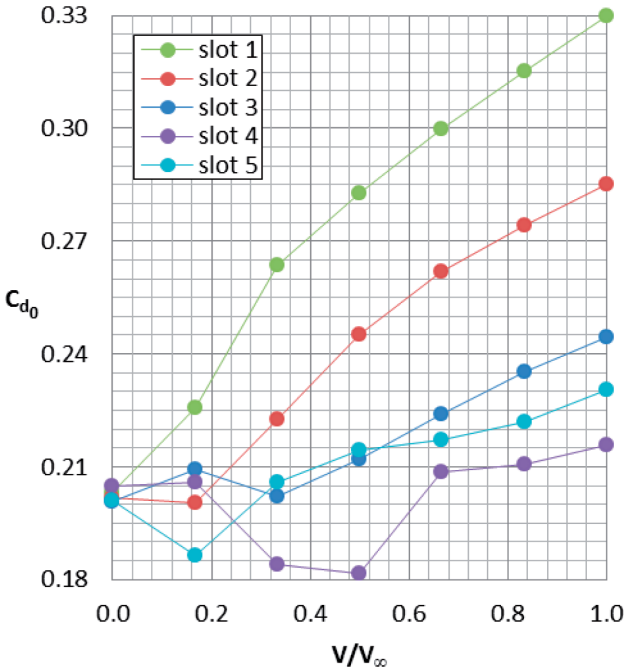

Fig. 14. Calculated drag coefficient at 21° of incidence

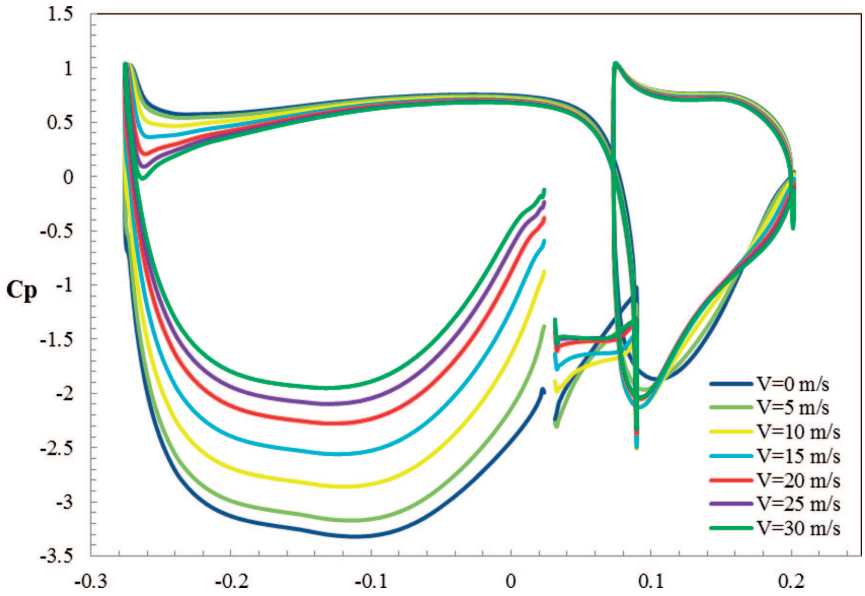

Fig. 15. Calculated surface pressure coefficient distribution over the wing at 11° of incidence with active slot 1

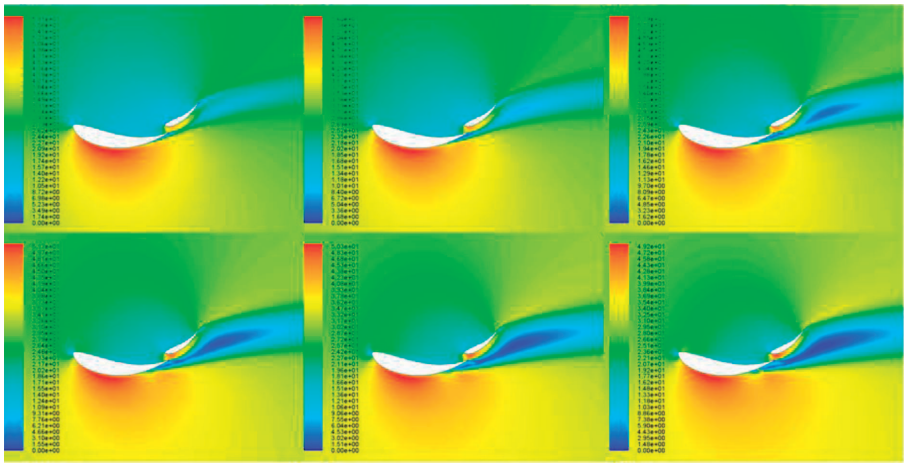

Fig. 16. Computed contours of air velocity around the wing profile at 11° of incidence for slot 1 active

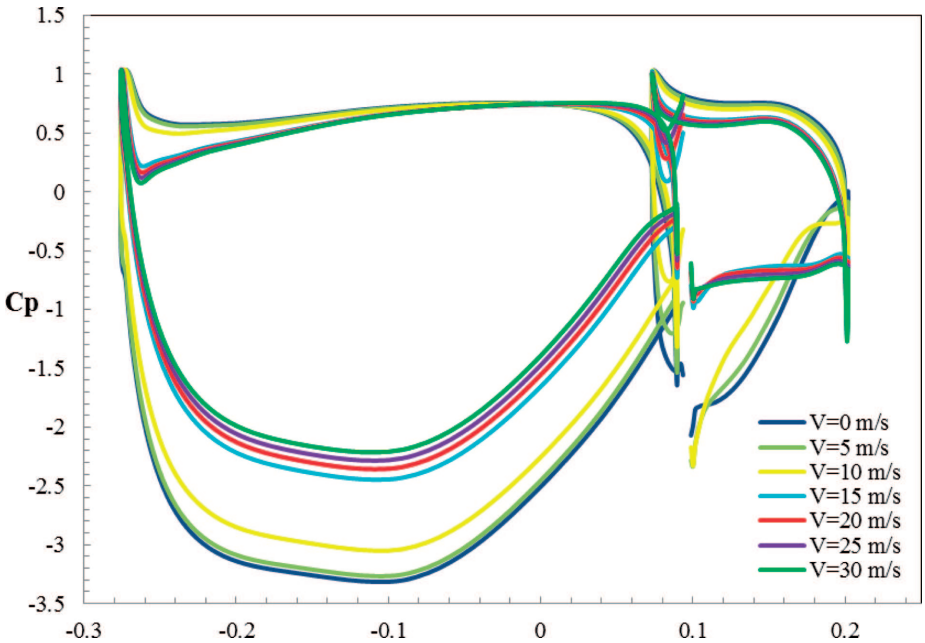

Fig. 17. Calculated surface pressure coefficient distribution over the wing at 11° of incidence for slot 5 active

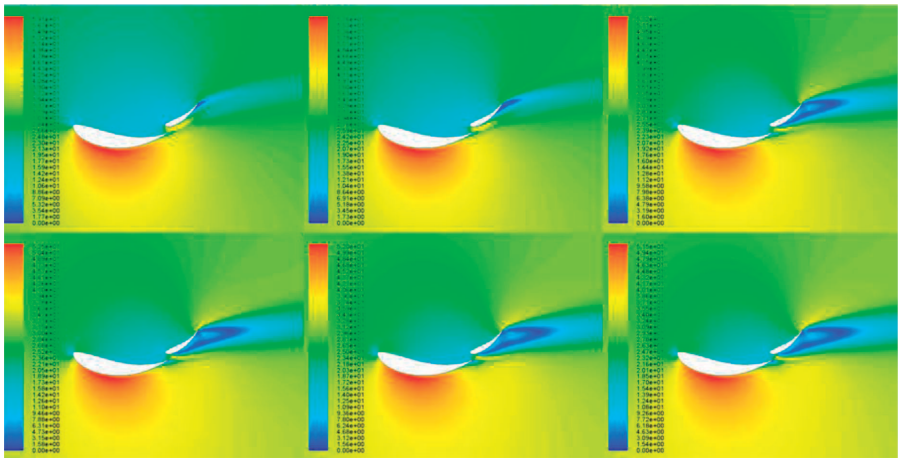

Fig. 18. Computed contours of air velocity around the wing profile at 11° of incidence for slot 5 active

For both angles of attack, the air injected through slots located on the main profile increased the drag coefficient significantly due to the velocity of the air flow from the outlet altering the flow over the wing, as shown in Figure 13 and 14. This increase is associated with the pressure drag produced in the area of separation. Therefore, for both angles of attack, the largest drag and the greatest decrease in lift force was obtained for slot 1, because it was located closer to the leading edge and the length of the section where separation occurs was the greatest one.

The curves of downforce coefficient for the air jets located on the additional profile, shown in Figures 11 and 12, are characterized by a rapid decrease after a certain value of the duct outlet velocity was reached, which was unique for each case. This velocity was related to the occurrence of flow separation on the secondary element. Figure 17 shows the pressure distribution over the profile for slot 5 at 11^o of incidence. It can be noticed that the pressure on the lower edge of the main element increases with the slot air velocity, but this rise has initiated from the velocity value at which separation occurs and causes stall. For inlets situated on the flap, this effect does not take place for the low air slot velocity, which is in contrast to slots located at the main element where separation occurs from the onset. The stall on the additional element, as show in Figure 18, causes a small separation at the trailing edge. For both incidences, the greatest decrease in lift force is observed for slot 5.

For slots located on the additional profile, the drag coefficient behaves differently to the previous cases, as shown in Figure 13 and 14. For low velocity decreases, the value of the coefficient for slot 5 at both angles of attack considered remains almost constant, but it is followed by a gradual

rise with an increase in the additional air stream velocity. The increase of drag is associated with a sharp drop in value of the downforce coefficient caused by a stall. The curves of drag coefficient for slot 4 behave similarly. However, initially there is a slight growth in value observed.

7. Induced drag coefficient

The total drag of a finite wing consists of the pressure and the viscous drag for a two-dimensional wing profile and additionally of wing tip vortex-induced drag. Therefore, all of these components were included. The induced drag values depend on the intensity of the vortices, which are determined by the value of downforce produced, and are therefore estimated by the approximate formula [1]:

$$C_{d_i} = \frac{C_l^2}{\pi\lambda}$$

where λ is a wing aspect ratio. This value, considered for a wing with end plates, was determined by applying the formula suggested by Hoerner [1]:

$$\lambda = \frac{b}{c\left(1 + 1.9\frac{h}{b}\right)}$$

where the wing span b and the chord c were 1 m and 0.5 m respectively, and the edge plate height h was 1 m.

The formula describing the induced drag is derived for the attached flow and is not fully valid for the separated flow case. Due to that fact, the following consideration shows only the aproximate drag reduction values.

The value of the total drag coefficient varied with the slot air velocity for both angles of attack, as shown in Figure 19 and 20. As it was previously done, the jet air velocity, was expressed in relation to the free stream velocity. Since the induced drag coefficient depended on the values ??of the downforce generated by the wing, and other parameters remained constant, the characteristic was exactly the same. The lowest drag for both angles of attack was obtained for slot 1 located on the main profile, and for slot 5, which was situated on the flap.

The ratio of the induced drag to the profile drag varied with slot air velocity for both angles of attack. To show the scale of the induced drag, this ratio is shown in Figures 21 and 22. One can notice that the value of the induced drag that occurs in three-dimensional flow analysis is much greater than the profile drag caused by pressure and shear stresses. Consequently, the downforce on which the induced drag mainly depends causes a significant drag penalty.

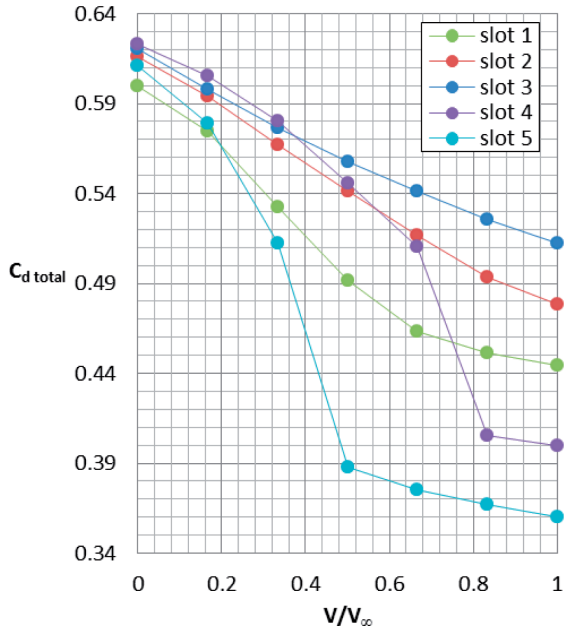

Fig. 19. Estimated total drag coefficient at 11° of incidence and different slots active

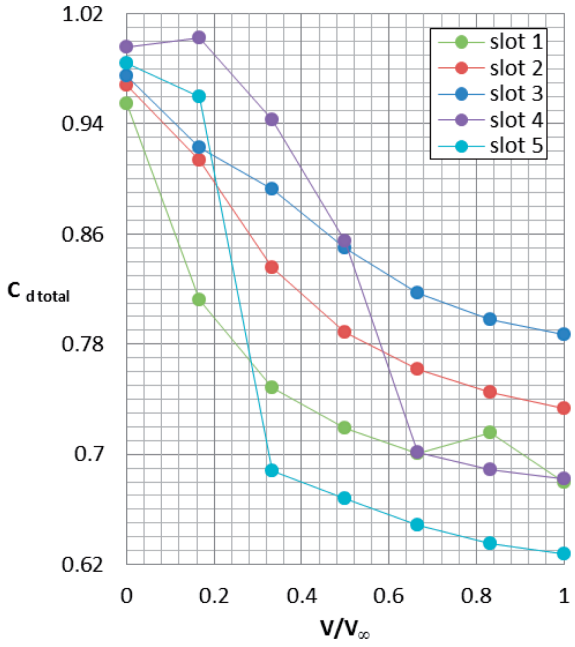

Fig. 20. Estimated total drag coefficient at 21° of incidence and different slots active

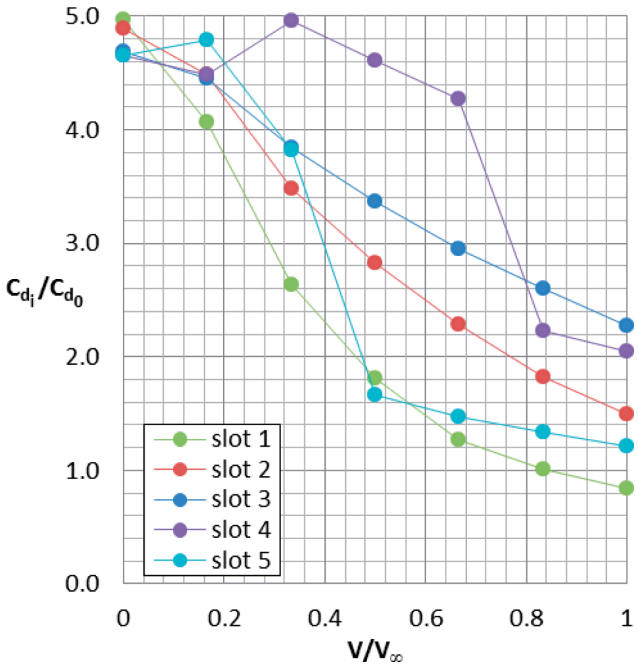

Fig. 21. Ratio of estimated induced drag values to calculated profile drag values at 11° of incidence

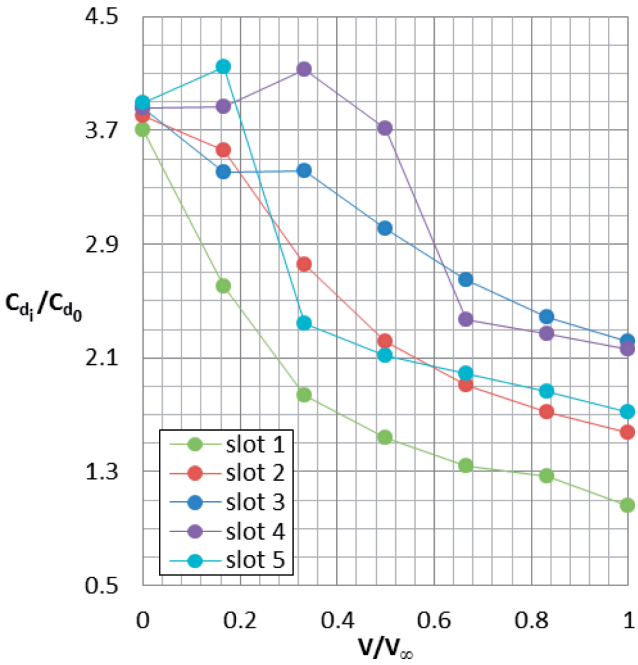

Fig. 22. Ratio of estimated induced drag values to calculated profile drag values at 21° of incidence

8. Conclusion

The numerical simulation was conducted for two-dimensional model of a two-element wing profile, including slots, that was designed for the Formula Student race. The investigation was conducted for 5 different slot locations with variation of its air outlet velocity at two incidences equal to 11° and 21°. Firstly, collated results confirmed that forcing separation through altering the flow over the wing by introducing the air stream from slots affects the wing in such a way that it enters a stalled state. Furthermore, two different flow separation structures have been recognised. Injections of air through slots located on the main airfoil element only cause separation on the main element, leaving the additional element with attached flow. This is unlikely to what is done by slots located at the additional airfoil element, which generate separation on both elements. In the 2D analysis, profile stall conditions were always correlated with an increase in the profile drag. Taking into account additional three-dimensional effects on a low aspect wing used in cars, stall conditions were accomplished by the reduction of total aerodynamic drag that were strongly affected by induced drag of vortical structures at the wing tips. Finally, if the flow over the wing is stalled, the result is a huge drop in the downforce coefficient resulting in total net drag reduction, even if the profile drag increases. This is the reason for major benefits in terms of the top speed of a racing car. It should be noted, however, that stalling the flap is more beneficial than the main wing stall. The investigation has shown that the optimal position of the duct outlet is slot 5, for which forced flow separation occurs at the lowest slot outlet air velocity.

Manuscript received by Editorial Board, May 18, 2012;
final version, March 12, 2013.

REFERENCES

[1] Katz J.: ***Race Car Aerodynamics. Designing for Speed***. *2nd. ed.* Cambridge, Bentley Publishers, 2006.
[2] Piechna J.: ***Podstawy aerodynamiki pojazdów.*** Warszawa, Wydawnictwo Komunikacji i Łączności, 2000.
[3] Abbott I. H., von Doenhoff A. E.: ***Theory of Wing Sections.*** New York, Dover Publications, 1959.
[4] Anderson J. J. D.: ***Fundamentals of Aerodynamics.*** 3rd. ed. New York, McGraw-Hill, 2001.
[5] Went J. F.: ***Computational Fluid Dynamics an Introduction.*** 3rd. ed. Springer, 2009.
[6] McLaren. http://www.mclaren.com/formula1/mp4-27. Internet web-site, accessed on 20/01/2013.

Numeryczne badanie sterowanego oderwania przepływu spowodowanego przez dodatkowe strumienie powietrza z dysz umieszczonych na skrzydle

S t r e s z c z e n i e

W artykule przedstawiono wyniki badań numerycznych zjawiska sterowanego oderwania przepływu na płacie dociskowym praktycznie wykorzystywanym w wyścigach Formuły 1 przez urządzenie o nazwie F-duct. Oderwanie przepływu zostało spowodowane wprowadzeniem zaburzenia poprzez strumień powietrza ze szczeliny, co doprowadziło do zmniejszenia całkowitego oporu aerodynamicznego płata dociskowego. Pozycje szczeliny i prędkość powietrza z nich wyrzucanego były głównymi parametrami kontrolującymi oderwanie przepływu. Głównym przedmiotem badań były: struktura przepływu, rozkłady ciśnienia na powierzchni profilu oraz generowane siły nośna i oporu. Podczas badań zostały rozpoznane dwie różne struktury oderwania przepływu. Zazwyczaj oderwanie przepływu na płacie związane jest ze wzrostem oporu profilowego. Jednak w przypadku trójwymiarowym dla płata o skończonej rozpiętości występuje dodatkowy składnik oporu ciśnieniowego spowodowany pojawieniem się wirów krawędziowych. Opór ten jest proporcjonalny do współczynnika siły docisku. Eksperyment pokazał, że oderwanie przepływu występujące na płacie dociskowym zwiększa opór profilowy, ale jednocześnie zmniejszając opór indukowany co w konsekwencji prowadzi do zmniejszenia całkowitego oporu aerodynamicznego.

THE ARCHIVE OF MECHANICAL ENGINEERING

VOL. LX 2013 Number 2

10.2478/meceng-2013-0014

Key words: flight dynamics, Flight Data Recorder, Levenberg-Marquardt Algorithm, Maximum Likelihood Estimation, Output Error Method, parametric identification

PIOTR LICHOTA [*], *MACIEJ LASEK* [*]

MAXIMUM LIKELIHOOD ESTIMATION FOR IDENTIFICATION OF AIRCRAFT AERODYNAMIC DERIVATIVES

This article investigates identification of aircraft aerodynamic derivatives. The identification is performed on the basis of the parameters stored by Flight Data Recorder. The problem is solved in time domain by Quad-M Method. Aircraft dynamics is described by a parametric model that is defined in Body-Fixed-Coordinate System. Identification of the aerodynamic derivatives is obtained by Maximum Likelihood Estimation. For finding cost function minimum, Lavenberg-Marquardt Algorithm is used. Additional effects due to process noise are included in the state-space representation. The impact of initial values on the solution is discussed. The presented method was implemented in Matlab R2009b environment.

1. Introduction

The development of civil aviation is associated with permanent problem-solving in safety and economy. Determining changes in aerodynamic characteristics is one of the areas that could be used for both improving safety and lowering costs.

At present, there is a lack of effective methods allowing for determining changes in aerodynamic derivatives due to e.g. maintenance. In order to find out the values of various aerodynamic derivatives, an identification experiment could be performed. Such an approach is possible, however, because of valid regulations, is highly unprofitable. Identification experiment costs would be higher than possible profits (e.g. due to maintenance program changes). Therefore, in civil aircraft, this approach is used only for flight simulators – due to certification regulations.

A possible solution is to identify the aerodynamic characteristics on the basis of parameters that are registered during each scheduled flight by flight

[*] *The Institute of Aeronautics and Applied Mechanics, Warsaw University of Technology, Warsaw, Poland; E-mail: plichota@meil.pw.edu.pl*